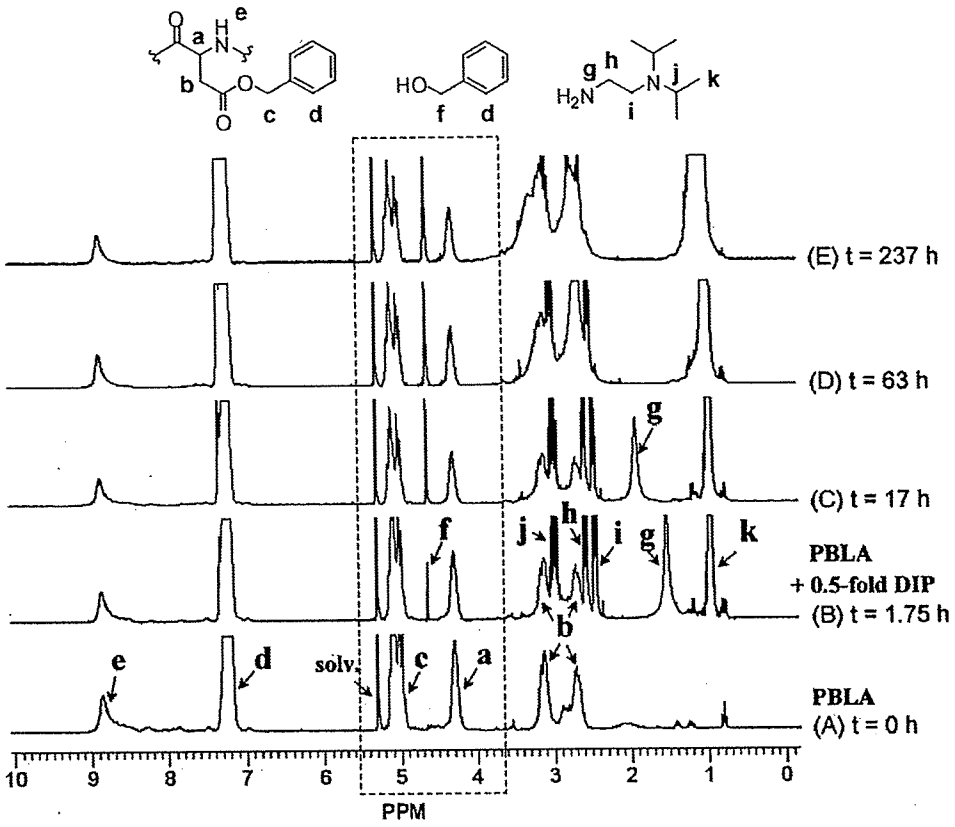

Fig. 5. Time-trace of ^{1}H NMR spectra of PBLA reacting with 0.5-fold DIP in CD_2Cl_2 at 35 °C.

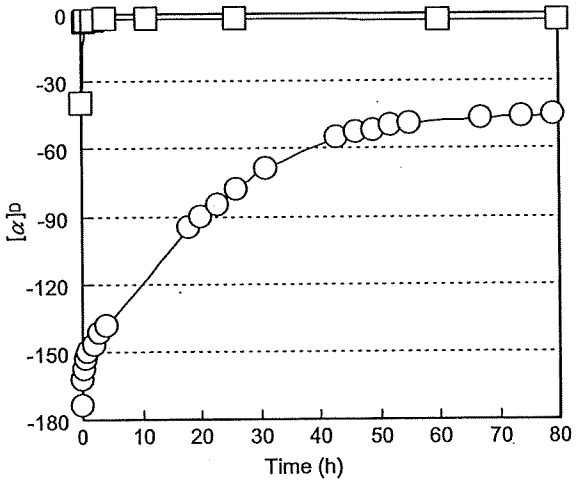

Fig. 6. Time-trace of $[\alpha]_D$ of PBLA reacting with 1-fold DIP at room temperature in DMSO (□) and CH_2Cl_2 (○).

zero after the DIP addition, suggesting the prompt racemization. $[\alpha]_D$ of PBLA in CH_2Cl_2 showed a highly negative value compared to that in DMSO due to the formation of the left-handed α-helix. Then, after the addition of DIP, alternatively, $[\alpha]_D$ of the system revealed a gradual shift in the positive direction and converged from the value of −180 to −45 after 80 h. It should be noted that the $[\alpha]_D$ value of −45 coincided with that for the random coiled PBLA in polar solvents such as DMSO.

Further analysis revealed that racemization occurred in the polar solvents and was effectively prohibited in the apolar solvents (Table 1), indicating that the $k_{2\_apolar\ solvent}$ was quite smaller than the $k_{2\_polar\ solvent}$. It is worth mentioning that the optical purity of the L-isomers was maintained with the yield of 95% in CH_2Cl_2, which is unprecedentedly high.

Racemization occurs by the rearrangement of the eliminated proton in the α position from Si face known as the keto–enol tautomerization (Scheme 2). It is reasonable to assume that the keto–enol tautomerzation is thermodynamically easy to occur in the polar solvents and not in the apolar solvents. Therefore, the racemization was effectively prohibited in the apolar solvents. Furthermore, the secondary structure of the polymer strands may also be a factor affecting racemization. The formation of an enol structure may be restricted in the α-helical structure because of the

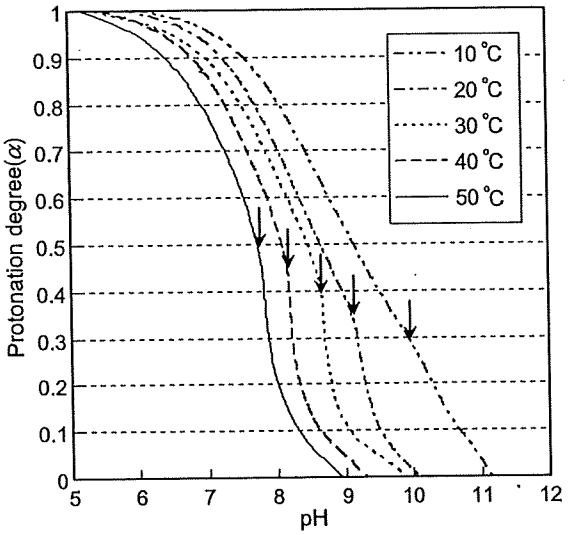

Fig. 7. Protonation degree (α) as a function of pH (α/pH curve) for PAsp(DIP) prepared in DMF. Each arrow in the figure indicates the pH at which the transmittance of the polymer solution decreased to 95%.

intramolecular hydrogen bond. However, further analyses may be needed to clearly explain the reaction scheme.

3.5. Solution properties of PAsp(DIP)

The analysis of the aqueous solution property of PAsp(DIP) synthesized in DMF was performed by the potentiometric titration and transmittance measurement to obtain α–pH curves at various temperatures (Fig. 7). The transmittance sharply decreased at a specific pH for all of the measuring temperatures, suggesting that the polymer became hydrophobic with the deprotonation to precipitate out of the solution.

The apparent pK_a ($pK_{a,app}$) values defined as a pH of $\alpha = 0.5$ increased with the decrease of the temperature from $pK_{a,app} = 7.7$ at 50 °C to $pK_{a,app} = 9.3$ at 10 °C. These results indicate that at a higher temperature, PAsp(DIP) is more liable to release proton because it is energetically preferable for the amphiphilic polycations to release highly condensed protons on the polymer strand to form the collapsed globule. However, stabilization due to the hydrophobic hydration was promoted at a lower temperature to maintain the solubility of PAsp(DIP) even at the higher range of pH. Eventually, PAsp(DIP) will be feasible to use as a novel smart materials with dual sensitivity i.e., sensitivity to both pH and temperature.

4. Conclusion

It was revealed that the aminolysis of PBLA, which proceeds involving a succinimide intermediate, was useful for quantitatively introducing the functional group into the side chain of PBLA. Moreover, racemization was effectively suppressed through the aminolysis in CH_2Cl_2 to give polyaspartamide with an appreciably high optical purity of 95%. This optical purity will apparently be a great advantage in its application as biomaterials. The cationic PAsp(DIP) synthesized by this method showed the dual sensitivity to pH and temperature, and thus may have a potential utility as novel smart biomaterials. In conclusion, this method of aminolysis is a simple and efficient way of constructing a polyaspartamide library from PBLA as a single platform polymer, and can be applied for screening the various utilities of structurally well-defined polyaspartamide derivatives as functionality materials.

Acknowledgements

The authors wish to express their gratitude to Prof. T. Tsuruta, Professor Emeritus, The University of Tokyo, for his valuable discussions and critical comments on this research. This work was financially supported by the Core Research for Evolutional Science and Technology (CREST) from the Japan Science and Technology Agency (JST).

References

[1] S. Jean-Claude, B. Jean-Claude, React. Polym. 12 (1990) 3.
[2] S. Jean-Claude, B. Jean-Claude, React. Polym. 12 (1990) 133.
[3] S. Jean-Claude, B. Jean-Claude, React. Polym. 13 (1990) 1.
[4] R. Arshdy, Adv. Polym. Sci. 111 (1994) 1.
[5] H. Mao, C. Li, Y. Zhang, S. Furyk, P.S. Cremer, D.E. Bergbreiter, Macromolecules 37 (2004) 1031.
[6] A. Godwin, M. Hartenstein, A.H.E. Müller, S. Brocchini, Angew. Chem. Int. Ed. 40 (2001) 594.
[7] W. Wu, B. Jin, G. Krippner, K. Watson, Bioorg. Med. Chem. Lett. 10 (2000) 341.
[8] L.E. Strong, L.L. Kiessling, J. Am. Chem. Soc. 121 (1999) 6193.
[9] A. Carrillo, K. Gujraty, P. Rai, R. Kane, Nanotechnology 16 (2005) S416.
[10] P. Strohriegl, Makromol. Chem. 194 (1993) 363.
[11] Y.S. Yang, G.R. Qi, J.W. Qian, S.L. Yang, J. Appl. Polym. Sci. 68 (1998) 665.
[12] Y.X. Liu, Z.J. Du, Y. Li, C. Zhang, C.J. Li, X.P. Yang, H.Q. Li, J. Appl. Polym. Sci. 44 (2006) 6880.
[13] R. Luxenhofer, R. Jordan, Macromolecules 39 (2006) 3509.

[14] B. Parrish, R.B. Breitenkamp, T. Emrick, J. Am. Chem. Soc. 127 (2005) 7404.
[15] T.J. Deming, Adv. Drug. Deliv. Rev. 54 (2002) 1145.
[16] S. Brocchini, Adv. Drug. Deliv. Rev. 53 (2001) 123.
[17] M. Ali, S. Brocchini, Adv. Drug. Deliv. Rev. 58 (2006) 1671.
[18] A. Lavasanifar, J. Samuel, G.S. Kwon, Adv. Drug. Deliv. Rev. 54 (2007) 169.
[19] G. Pratesi, G. Savi, G. Pezzoni, O. Bellini, S. Penco, S. Tinelli, F. Zunino, Brit. J. Cancer 52 (1985) 841.
[20] H.J.-P. Ryser, W.-C. Shen, Proc. Natl. Acad. Sci. USA 75 (1978) 3867.
[21] G.Y. Wu, C.H. Wu, J. Biol. Chem. 262 (1987) 4429.
[22] N. Lupu-Lotan, A. Yaron, A. Berger, M. Sela, Biopolymers 3 (1965) 625.
[23] A.D. Marre, H. Soyez, E. Schacht, J. Pytela, Polymer 35 (1994) 2443.
[24] M.G. Meirim, E.W. Neuse, F. Parisi, Angew. Makromol. Chem. 175 (1990) 141.
[25] E.W. Neuse, A.G. Perlwitz, S. Schmitt, Angew. Makromol. Chem. 181 (1990) 153.
[26] E.W. Neuse, A.G. Perlwitz, S. Schmitt, Angew. Makromol. Chem. 192 (1991) 35.
[27] E.W. Neuse, B.B. Patel, C.W.N. Mbonyana, J. Inorg. Organomet. Polym. 1 (1991) 147.
[28] J.C. Swarts, E.W. Neuse, G.J. Lamprecht, J. Inorg. Organomet. Polym. 4 (1994) 143.
[29] R.W. Niven, F. Rypacek, P.R. Byron, Pharm. Res. 7 (1990) 990.
[30] M. Schwamborn, Polym. Degrad. Stab. 59 (1998) 39.
[31] K.C. Low, A.P. Wheeler, L.P. Koskan, Adv. Chem. Ser. 248 (1996) 99.
[32] T. Nakato, M. Yoshitake, K. Matsubara, M. Tomida, T. Kakuchi, Macromolecules 31 (1998) 2107.
[33] S.K. Wolk, G. Swift, H.-P. Yi, K.M. Yocom, R.L. Smith, E.S. Simon, Macromolecules 27 (1994) 7613.
[34] K. Itaka, N. Kanayama, N. Nishiyama, W.-D. Jang, Y. Yamasaki, K. Nakamura, H. Kawaguchi, K. Kataoka, J. Am. Chem. Soc. 126 (2004) 13612.
[35] S. Fukushima, K. Miyata, N. Nishiyama, N. Kanayama, Y. Yamasaki, K. Kataoka, J. Am. Chem. Soc. 127 (2005) 2810.
[36] Y. Bae, W.-D. Jang, N. Nishiyama, S. Fukushima, K. Kataoka, Mol. Biosyst. 1 (2005) 242.
[37] A. Koide, A. Kishimura, K. Osada, W.-D. Jang, Y. Yamasaki, K. Kataoka, J. Am. Chem. Soc. 128 (2006) 5988.
[38] N. Kanayama, S. Fukushima, N. Nishiyama, K. Itaka, W.-D. Jang, K. Miyata, Y. Yamasaki, U.-I. Chung, K. Kataoka, Chem. Med. Chem. 1 (2006) 439.
[39] Arnida, N. Nishiyama, N. Kanayama, W.-D. Jang, Y. Yamasaki, K. Kataoka, J. Control. Release 115 (2006) 208.
[40] H.G. Schild, Prog. Polym. Sci. 17 (1992) 163.
[41] D.D. Perrin, W.L.F. Armarego, D.R. Perrin, Purification of Laboratory Chemicals, Pergamon, Oxford, 1980.
[42] K. Nokihara, J. Gerhardt, Chirarity 13 (2001) 431.
[43] P. Dubin, F.E. Karasz, Biopolymer 11 (1972) 1745.
[44] R.H. Karlson, K.S. Norland, G.D. Fasman, E.R. Blout, J. Am. Chem. Soc. 82 (1960) 2268.
[45] E.R. Blout, Biopolymers Symp. 1 (1964) 397.
[46] A.J. Adler, G.D. Fasman, E.R. Blout, J. Am. Chem. Soc. 85 (1963) 90.
[47] C.G. Swain, J.F. Brown, J. Am. Chem. Soc. 74 (1952) 2538.
[48] J.L. Radkiewicz, H. Zipse, S. Clarke, K.N. Houk, J. Am. Chem. Soc. 118 (1996) 9148.
[49] G.G. Smith, G.V. Reddy, J. Org. Chem. 54 (1989) 4529.
[50] T. Takata, T. Shimo-Oka, K. Miki, N. Fujii, Biochem. Biophys. Res. Commun. 334 (2005) 1022.
[51] N. Fujii, K. Harada, Y. Momose, N. Ishii, M. Akaboshi, Biochem. Biophys. Res. Commun. 263 (1999) 322.
[52] N. Fujii, L.J. Takemoto, Y. Momose, S. Matsumoto, K. Hiroki, M. Akaboshi, Biochem. Biophys. Res. Commun. 265 (1999) 746.
[53] A.C.T. Van Duin, M.J. Collins, Org. Geochem. 29 (1998) 1227.
[54] T. Nakato, A. Kusuno, T. Kakuchi, J. Polym. Sci. Part A: Polym. Chem. 38 (2000) 117.

Available online at www.sciencedirect.com
ScienceDirect
Journal of Controlled Release 121 (2007) 146–155
journal of controlled release
www.elsevier.com/locate/jconrel

Optimization of (1,2-diamino-cyclohexane)platinum(II)-loaded polymeric micelles directed to improved tumor targeting and enhanced antitumor activity

Horacio Cabral [a], Nobuhiro Nishiyama [b], Kazunori Kataoka [a,b,c,*]

[a] *Department of Materials Engineering, Graduate School of Engineering, The University of Tokyo, 7-3-1 Hongo, Bunkyo-ku, Tokyo 113-8656, Japan*
[b] *Center for Disease Biology and Integrative Medicine, Graduate School of Medicine, The University of Tokyo, 7-3-1 Hongo, Bunkyo-ku, Tokyo 113-0033, Japan*
[c] *Center for NanoBio Integration, The University of Tokyo, 7-3-1 Hongo, Bunkyo-ku, Tokyo, 113-8656, Japan*

Received 19 March 2007; accepted 21 May 2007
Available online 29 May 2007

Abstract

Polymeric micelles are promising nanocarriers, which might enhance the efficacy of antitumor drugs. Herein, polymeric micelles incorporating dichloro(1,2-diamino-cyclohexane)platinum(II) (DACHPt), the oxaliplatin parent complex, were prepared through the polymer-metal complex formation of DACHPt with poly(ethylene glycol)-*b*-poly(glutamic acid) [PEG-*b*-P(Glu)] block copolymer having different lengths of the poly (glutamic acid) block [p(Glu): 20, 40, and 70 U]. The resulting micelles were studied with the aim of optimizing the system's biological performance. DACHPt-loaded micelles (DACHPt/m) were approximately 40 nm in diameter and had a narrow size distribution. *In vivo* biodistribution and antitumor activity experiments (CDF_1 mice bearing the murine colon adenocarcinoma C-26 inoculated subcutaneously) showed 20-fold greater accumulation of DACHPt/m at the tumor site than free oxaliplatin to achieve substantially higher antitumor efficacy. Moreover, the micelles prepared from PEG-*b*-P(Glu) with 20 U of P(Glu) exhibited the lowest non-specific accumulation in the liver and spleen to critically reduce non-specific accumulation, resulting in higher specificity to solid tumors. The antitumor effect of DACHPt/m was also evaluated on multiple metastases generated from intraperitoneally injected bioluminescent HeLa (HeLa-Luc) cells. The *in vivo* bioluminescent data indicated that DACHPt/m decreased the signal 10-to 50-fold compared to the control indicating a very strong antitumor activity. These results suggest that DACHPt/m could be an outstanding drug delivery system for oxaliplatin in the treatment of solid tumors.

Keywords: Polymeric micelles; DACHPt; Oxaliplatin; Biodistribution; Antitumor activity

1. Introduction

Oxaliplatin, oxalato(trans-*l*-1,2-diaminocyclohexane)platinum(II), is a third-generation platinum drug approved by the United States Food and Drug Administration in 2004 for the first-line treatment of advanced colorectal cancer in combination with 5-fluorouracil/folinic acid (5-FU/LV) [1]. The incorporation of oxaliplatin into the colorectal cancer program represents a major improvement in the treatment of the disease. The synergistic effects between oxaliplatin and 5-FU/LV significantly increased the response rates, improved the time-sensitive response parameters, and contributed to the removal of heretofore unresectable hepatic metastases, thereby changing the natural history of the malignancy. Nevertheless, oxaliplatin distributes rapidly to the whole body and, even though it shows better tolerability relative to other platinum drugs, cumulative peripheral distal neurotoxicity and acute dysesthesias restrain the range of working doses [2,3]. Consequently, enormous effort has been dedicated to develop drug delivery systems that increase the blood residence time of oxaliplatin and other platinum drugs, and target those drugs to solid tumors by taking advantage of the enhanced permeability and retention (EPR) effect [4]. Liposomes and macromolecular carriers (water soluble polymer–drug conjugates) have been the first attempts

* Corresponding author. Department of Materials Engineering, Graduate School of Engineering, The University of Tokyo, 7-3-1 Hongo, Bunkyo-ku, Tokyo 113-8656, Japan. Tel.: +81 3 5841 7138; fax: +81 3 5841 7139.
E-mail address: kataoka@bmw.t.u-tokyo.ac.jp (K. Kataoka).

0168-3659/$ - see front matter © 2007 Elsevier B.V. All rights reserved.
doi:10.1016/j.jconrel.2007.05.024

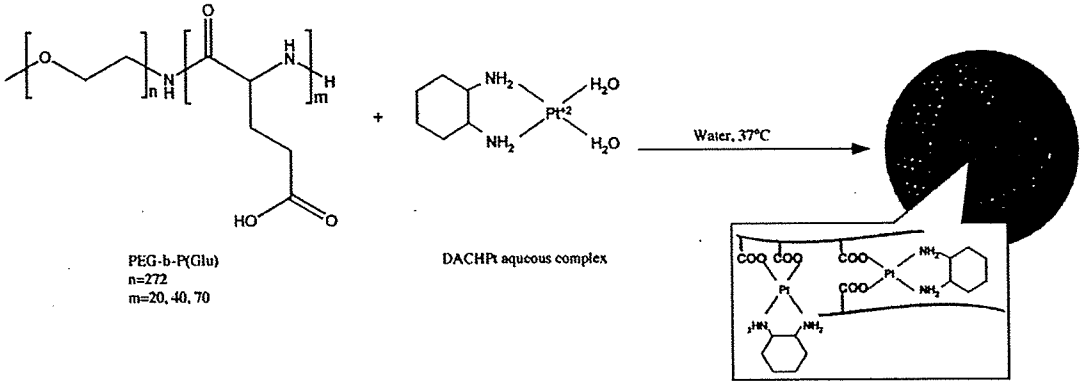

Fig. 1. Formation of DACHPt-loaded micelle (DACHPt/m).

to be considered [5–11]. However, successful formulations have not been developed yet due to unfavorable properties of platinum drugs. For example, the low water solubility of platinum drugs limits their loading efficacy into liposomal formulations (only 1 to 7% of drug loading). Moreover, liposomes incorporating the drug in the lipid bilayer showed rapid leakage of the drugs during storage and in the bloodstream [6]. In the case of macromolecular-drug formulations at high substitution ratios, they show reduced solubility due to the enlarged cohesive forces and to the cross-linking formation between polymer chains [8].

A novel approach to the design of nanocarriers for platinum drugs has been utilizing polymeric micelles [12–15]. Polymeric micelles present unique advantages over other types of drug-carrier systems: (i) prolonged blood circulation due to the efficient stealthy behavior of the dense shell of poly(ethylene glycol) (PEG), which hinders the adsorption of plasma proteins on the surface of the nanostructure and avoids recognition by the reticuloendothelial system (RES); (ii) easiness in encapsulating different compounds by modulating the micelle-forming block copolymers; (iii) reduced cumulative toxicity because of the micellar self-dissociation into unimers with molecular weight lower than that of the threshold of glomerular excretion; (iv) simplicity in size control by changing the chemical composition of block copolymers; (v) deeper tumor penetration due to the sub-100 nm size; (vi) facile management of the drug release in a controlled and environment-sensitive manner by modification of the drug-polymer system; and (vii) improved targeting capability by conjugating pilot molecules on the surface of micelles.

The first generation of platinum-drug-loaded micelles was prepared by the metal-complex formation between cis-dichlorodiammineplatinum(II) (cisplatin, CDDP) and poly(ethylene glycol)-*b*-poly(amino acid) block copolymers [16–21]. The exceptional physicochemical and biological properties of the CDDP-loaded micelle indicate them as an outstanding delivery system for CDDP complexes and a phase I clinical trial is being performed in United Kingdom (NC-6004, Nanocarrier, Japan). More recently, new platinum-drug-loaded polymeric micelles incorporating the oxaliplatin active complex were prepared by the complexation of dichloro(1,2-diaminocyclohexane)platinum(II) (DACHPt) with PEG-*b*-P(Glu) [22]. Previous studies demonstrated that the DACHPt-loaded micelle (DACHPt/m) might maintain its micellar structure for approximately 10 days in 10 mM PBS plus 150 mM NaCl, considerably longer than the stability of the CDDP-loaded micelles (ca 50 h) under the same conditions, while the drug was released from the micelle core in a sustained manner. Moreover, DACHPt/m showed remarkably prolonged blood circulation and more than 20-fold greater accumulation in tumor tissue compared to free oxaliplatin. According to these results, DACHPt/m seems to be an exceptionally promising carrier for the active complexes of oxaliplatin.

Herein, the *in vitro* and *in vivo* biological properties of DACHPt/m prepared with poly(ethylene glycol)-*b*-poly(glutamic acid) [PEG-*b*-P(Glu)] were studied with the aim of optimizing the biological performance of the micelle. Thus, PEG-*b*-P(Glu) having different P(Glu) block lengths (20, 40, and 70 U) were synthesized and used for the micelle preparation. DACHPt/m was phisicochemically characterized to determine the size, size distribution, zeta-potential, drug loading, and weight fraction of block copolymer. The *in vivo* behavior of DACHPt/m was assessed by the biodistribution and antitumor activity experiments using CDF_1 mice bearing the murine colon adenocarcinoma 26 (C-26). Although oxaliplatin had shown low efficacy against this tumor model [23], we found that DACHPt/m considerably increased the antitumor activity of the drug, probably by maintaining high drug levels within the tumor for a prolonged period. Furthermore, since chemotherapy is used in patients with metastatic disease and all the established therapies reveal poor efficiency at the late stage of the disease [24], new therapeutic strategies are urgently needed. Moreover, given that the very low prognosis of late-stage cervical carcinoma [25] (5 years after treatment 15% or fewer of women with stage IV cancer survive) is mainly due to metastasis to the abdomen or the lungs, the antitumor activity of DACHPt/m was evaluated against a bioluminescent intraperitoneal metastatic tumor model of cervical cancer.

2. Experimental

2.1. Materials

γ-benzyl L-glutamate was purchased from Sigma Chemical (St. Louis, MO). Bis(trichloromethyl)carbonate (triphosgene) was purchased from Tokyo Kasei Kogyo (Tokyo, Japan). *N,N-*

Table 1
DACHPt-loaded micelles (DACHPt/m) size, zeta-potential and drug loading

Micelle formulation	Size(nm)	Zeta-potential(mV)	Drug loading, [DACHPt]/[Glu]
DACHPt/m 12–20	37	−3	0.317
DACHPt/m 12–40	40	−4	0.323
DACHPt/m 12–70	41	−4	0.288

dimethylformamide (DMF) and 3-(4,5-dimethylthiazol-2-yl)-2,5-diphenyltetrazolium bromide (MTT) were obtained from Wako Pure Chemical (Osaka, Japan). Dichloro(1,2-diamminocyclohexane)platinum(II) (DACHPt) and $AgNO_3$ were purchased from Aldrich Chemical (Milwaukee, WI). α-methoxy-ω-aminopoly(ethylene glycol) (CH_3O–PEG–NH_2; Mw= 12,000) was purchased from Nippon Oil and Fats (Tokyo, Japan).

2.2. Cell lines and animals

Murine colon adenocarcinoma 26 (C-26) cells were kindly supplied by the National Cancer Center (Tokyo, Japan). C-26 cells were maintained in RPMI 1640 medium (Sigma Chemical) containing 10% fetal bovine serum in a humidified atmosphere containing 5% CO_2 at 37 °C. Bioluminescent HeLa (HeLa-Luc) cells were purchased from Xenogen (Alameda, CA). Luciferase stable-HeLa-Luc cells were maintained in Dulbecco's Modified Eagle Medium (Sigma Chemical Co., Inc.) containing 10% fetal bovine serum in a humidified atmosphere containing 5% CO_2 at 37 °C for no more than two weeks to assure luciferase luminescence stability.

Table 2
Accumulation ratios and area under the curve (AUC) ratios between tumor and normal organs at 48 h after administration of DACHPt-loaded micelles (DACHPt/m)[a] prepared with PEG-*b*-P(Glu) 12–40 and free oxaliplatin

Drug	Accumulation ratio				AUC ratio[b]	
	Tumor/ liver	Tumor/ spleen	Tumor/ kidney	Tumor/ liver	Tumor/ spleen	Tumor/ kidney
DACHPt/m 12–40	1.25	1.26	3.9	1.25	1.53	3.12
Oxaliplatin	0.9	0.18	0.42	1.1	0.32	0.9

[a] Dose: 0.1 mg per mouse on Pt basis.
[b] AUC calculated by trapezoidal rule up to 48 h.

Severe Combined Immunodeficiency (SCID) and CDF_1 mice (female; 18–20 g body weight; 6 weeks old) were purchased from Charles River Japan (Kanagawa, Japan). All animal experiments were carried out in accordance with the Guide for the Care and Use of Laboratory Animals as stated by the NIH. Sterile procedures were followed to assure that SCID mice were disease-free.

2.3. Preparation of PEG-b-P(Glu)

PEG-*b*-P(Glu) block copolymers were synthesized in accordance with the previously described synthetic method

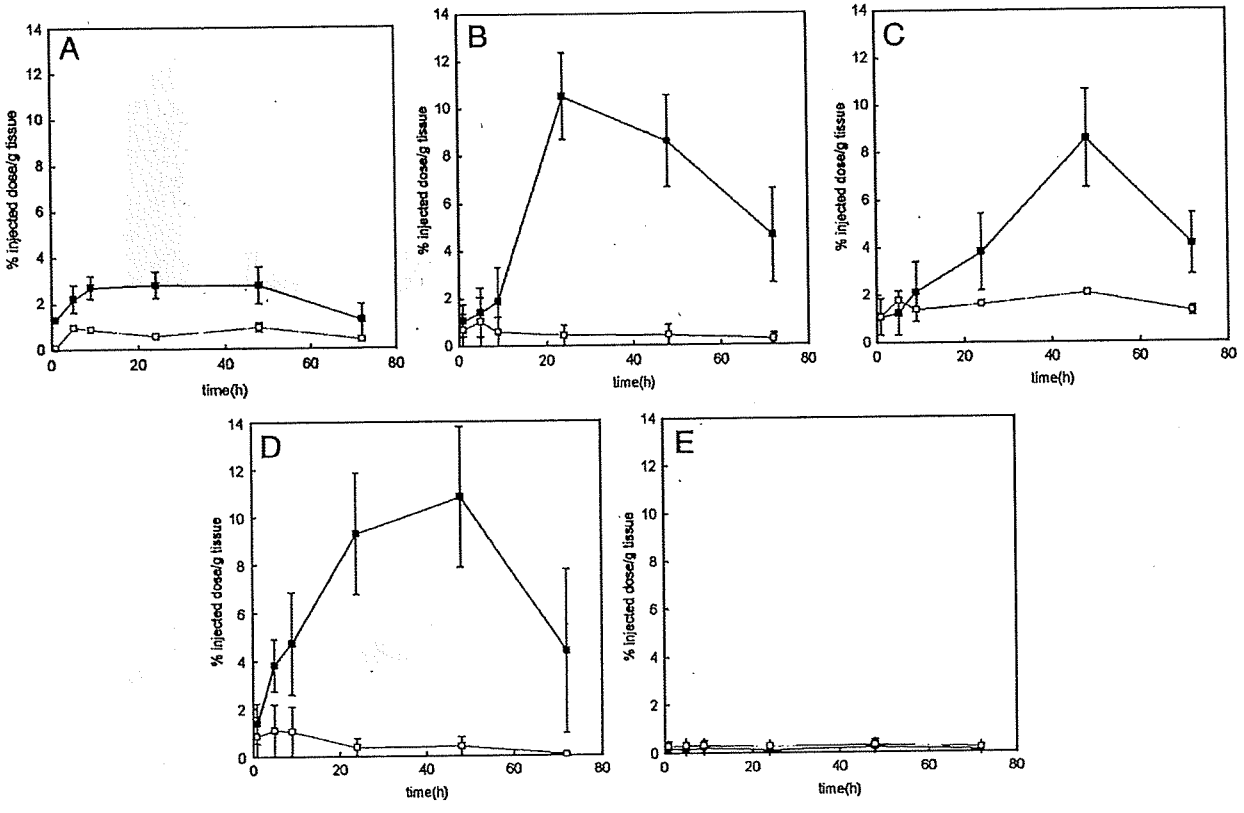

Fig. 2. Biodistribution of oxaliplatin (□) and DACHPt-loaded micelle (DACHPt/m) prepared with PEG-*b*-P(Glu) 12–40 (■): A. Kidney; B. Liver; C. Spleen; D. Tumor; E. Muscle. Data are expressed as averages±S.D.

[20] with a minor modification. Briefly, the *N*-carboxy anhydride of γ-benzyl L-glutamate was synthesized by the Fuchs–Farthing method using triphosgene. Then, *N*-carboxy anhydride of γ-benzyl L-glutamate was polymerized in DMF, initiated by the primary amino group of CH_3O–PEG–NH_2, to obtain PEG-*b*-poly(γ-benzyl L-glutamate) (PEG-*b*-PBLG) block copolymer with different PBLG block lengths (20, 40, and 70 U). The molecular weight distribution of PEG-*b*-PBLG was determined by gel permeation chromatography [column: TSK-gel $G3000_{HHR}$, $G4000_{HHR}$ (Tosoh, Yamaguchi, Japan); eluent: DMF containing 10 mM LiCl; flow rate: 0.8 ml/min; detector: refractive index (RI); temperature: 25 °C]. The polymerization degree of PBLG was verified by comparing the proton ratios of methylene units in PEG (–OCH_2CH_2–: δ=3.7 ppm) and phenyl groups of PBLG (–$CH_2C_6H_5$: δ=7.3 ppm) in ^{1}H-NMR measurement [JEOL EX270 (JEOL, Tokyo, Japan); solvent: DMSO-d_6; temperature: 80 °C]. PEG-*b*-PBLG was deprotected by mixing with 0.5 N NaOH at room temperature to obtain PEG-*b*-P(Glu). Complete deprotection was confirmed by ^{1}H-NMR measurement (solvent: D_2O; temperature: 25 °C). The compositions of PEG-*b*-P(Glu) are abbreviated as PEG-*b*-P(Glu) 12–20, PEG-*b*-P(Glu) 12–40 and PEG-*b*-P(Glu) 12–70 for the different P(Glu) block lengths (20, 40, and 70 U, respectively).

2.4. Preparation of DACHPt-loaded micelles (DACHPt/m)

DACHPt/m were prepared according to a previously described method [22]. Briefly, DACHPt (5 mM) was suspended in distilled water and mixed with silver nitrate ([$AgNO_3$]/[DACHPt]=1) to form an aqueous complex. The solution was kept in the dark at 25 °C for 24 h. AgCl precipitates found after the reaction were eliminated by centrifugation. Afterward, the supernatant was purified by passage through a 0.22 μm filter. Then, PEG-*b*-P(Glu) 12–20, 12–40, or 12–70 ([Glu]=5 mmol/liter) was added to DACHPt aqueous complex solution ([DACHPt]/[Glu]=1.0) and reacted for 120 h to prepare DACHPt/m. The prepared micelles were purified by ultrafiltration [molecular weight cutoff size (MWCO): 100,000]. The size distribution of DACHPt/m was evaluated by the dynamic light scattering (DLS) measurement at 25 °C using a Photal DLS-7000 dynamic laser scattering spectrometer (Otsuka Electronics, Osaka, Japan). The zeta-potential of DACHPt/m was determined using a Zetasizer Nano ZS90 (Malvern Instruments, Worcestershire, United Kingdom). The Pt content of the micelles was determined by an ion coupled plasma-mass spectrometer (4500 ICP-MS; Hewlett Packard, Palo Alto, CA).

2.5. Biodistribution

In order to analyze the fate of oxaliplatin and DACHPt/m *in vivo*, CDF_1 mice (female, n=6) were injected subcutaneously with C-26 cells (1×10^6 cells/ml). Fourteen days later, oxaliplatin or DACHPt/m prepared with PEG-*b*-P(Glu) 12–40 were intravenously injected by the tail vein at a dose of 100 μg/mouse on a platinum basis. Mice were sacrificed after defined time periods (1, 4, 8, 24, 48, and 72 h).

To assess the effect of formulation on the tissue distribution, CDF_1 mice (female, n=6) bearing s.c. C-26 tumors were intravenously administered oxaliplatin or DACHPt/m prepared with PEG-*b*-P(Glu) with different P(Glu) lengths (20, 40, and

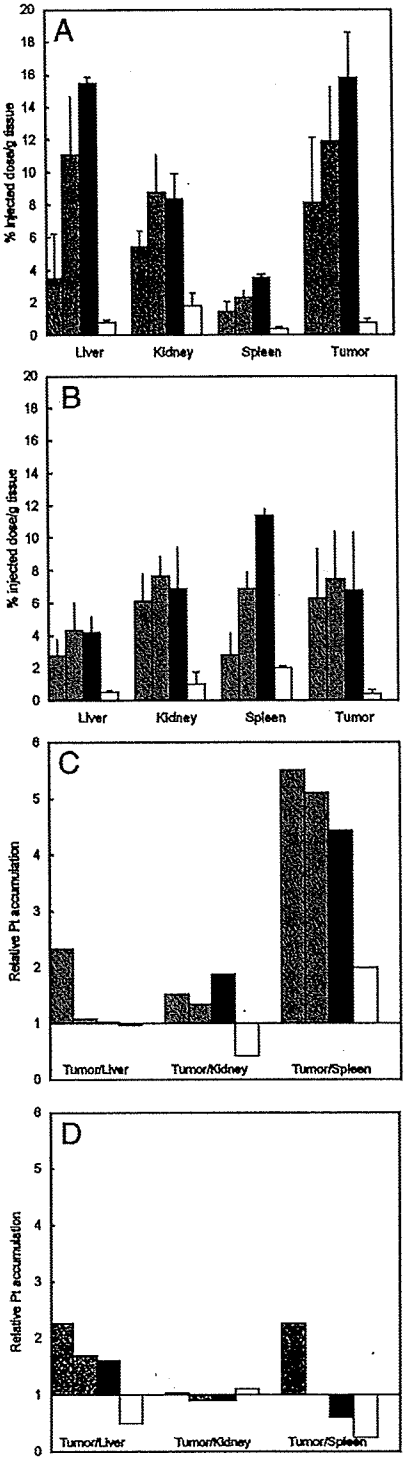

Fig. 3. Biodistribution of DACHPt-loaded micelle (DACHPt/m) prepared with PEG-*b*-P(Glu) 12–20(▨), PEG-*b*-P(Glu) 12–40(▨), PEG-*b*-P(Glu) 12–70(■) and oxaliplatin (□): A. 24 h; B.48 h; C. 24 h tumor/organ ratio; D. 48 h tumor/organ ratio. Data are expressed as averages±S.D.

70 U) at 100 μg/mouse on a platinum basis. Mice were sacrificed at 24 and 48 h post-incubation.

Tumor, liver, kidney, spleen, and muscle were collected. Blood was collected from the inferior vena cava, heparinized and centrifuged to obtain the plasma. Tissue samples were washed in ice-cold saline and weighed after removing excess fluid. All samples were dissolved in HNO_3 and evaporated to dryness. The Pt concentration was measured by ICP-MS after the samples were redissolved in 5 N HCl. The area under the curve (AUC) was calculated by the trapezoidal rule.

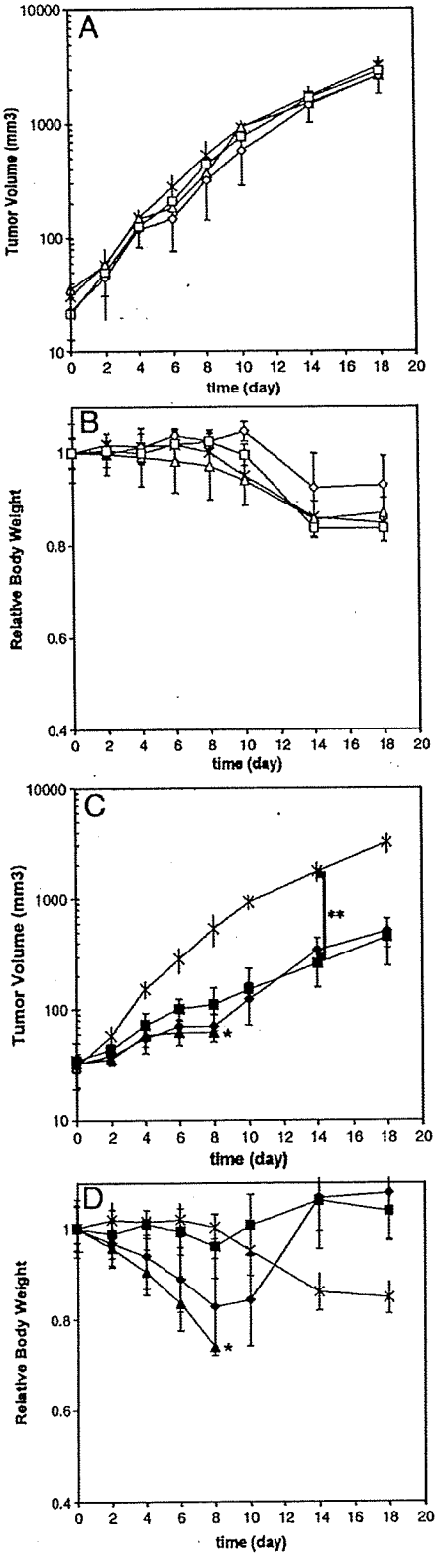

Fig. 4. Antitumor activity of DACHPt-loaded micelle (DACHPt/m) prepared with PEG-*b*-P(Glu) 12–40 against s.c. C-26 tumor model (n=5). Saline(×); oxaliplatin at 6 mg/kg(△); 4 mg/kg(◇); 2 mg/kg(□). DACHPt-loaded micelle (DACHPt/m) 12–40 at 6 mg/kg(▲); 4 mg/kg(◆); 2 mg/kg(■). A. Tumor volume (mm^3) for oxaliplatin treatment; B. Relative body weight of mice for oxaliplatin treatment; C. Tumor volume (mm^3) for DACHPt/m treatment; D. Relative body weight of mice for DACHPt/m treatment. Data are expressed as averages±S.D. *Toxic death. **$p<0.001$.

2.6. Antitumor activity assay

CDF_1 mice (female, n=6) were inoculated subcutaneously with C-26 cells (1×10^6 cells/ml). Tumors were allowed to grow for 1 week (the size of tumor at this point was approximately 30 mm^3 or 100 mm^3). Subsequently, mice were treated i.v. 4 times at 2-day intervals at doses of 2, 4, 6 and 10 mg/kg of oxaliplatin or 2, 4 and 6 mg/kg (on a platinum base) of DACHPt/m prepared with PEG-*b*-P(Glu) 12–20 or PEG-*b*-P (Glu) 12–40. The antitumor activity was evaluated in terms of tumor size (V), as estimated by the following equation:

$$V = a \times b^2/2$$

where a and b are the major and minor axes of the tumor measured by a caliper, respectively. The body weight was measured simultaneously and was taken as a parameter of systemic toxicity. The statistical analysis of animal data was carried out by the unpaired t-test.

2.7. Antitumor activity in a bioluminescent intraperitoneal metastasis model

SCID mice (female, n=5) were inoculated intraperitoneally with Hela-Luc cells (5×10^5 cells/ml). Tumors were allowed to grow for 3 days. Subsequently, mice were treated i.v. 3 times at 2-day intervals at doses of 4 and 6 mg/kg (on a platinum base) of oxaliplatin or DACHPt/m prepared with PEG-b-P(Glu) 12–20. *In vivo* bioluminescent imaging (BLI) was performed with an IVIS Imaging System (Xenogen) comprised of a highly sensitive, cooled CCD camera mounted in a light-tight specimen box. Images and measurements of bioluminescent signals were acquired and analyzed using Living Image software (Xenogen). Ten minutes prior to *in vivo* imaging, animals received the substrate D-luciferin (Biosynth) at 150 mg/kg in PBS by intraperitoneal injection and were anesthetized using 1–3% isoflurane (Abbott Laboratories, North Chicago, IL). Animals were placed onto a warmed stage inside the camera box and received continuous exposure to 1–2% isoflurane to sustain sedation during imaging. Imaging times ranged from 10 to 60 s, depending on the bioluminescence of the metastatic lesions. Five mice were imaged at a time. Tumor growth was monitored

by BLI every second day for 18 days. The light emitted from the bioluminescent tumors was detected *in vivo* by the IVIS Imaging System, was digitized and electronically displayed as a pseudocolor overlay onto a gray scale animal image. Regions of interest (ROI) from displayed images were drawn around the tumor sites and quantified as photons/second using the Living Image software. The statistical analysis of animal data was carried out by the unpaired *t*-test.

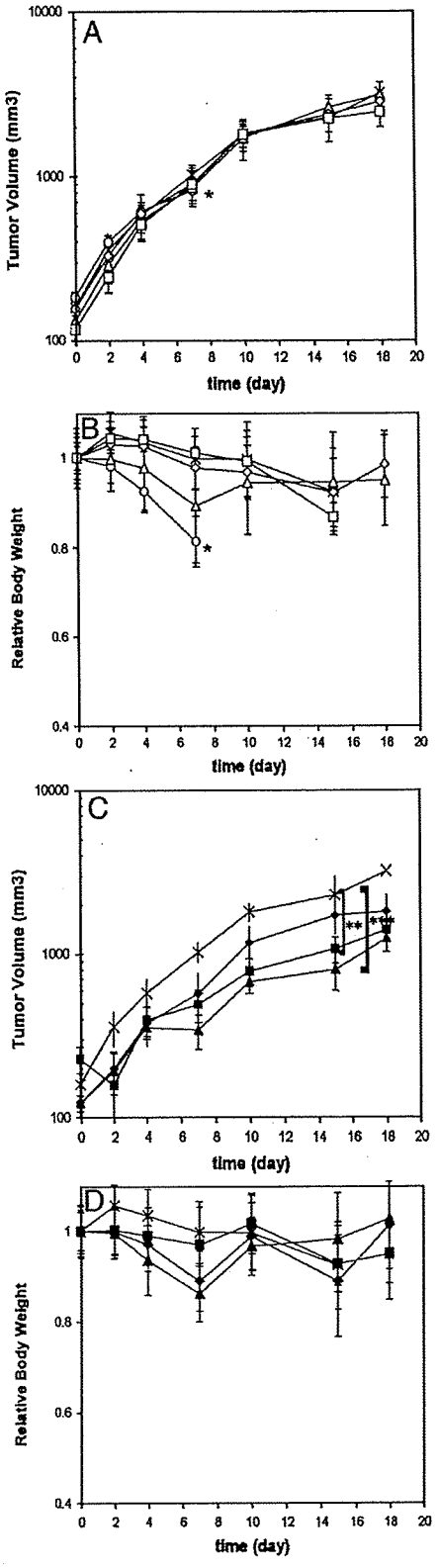

3. Results

3.1. Micelle characterization

The metal-polymer complex formation between DACHPt and the carboxylic group of the p(Glu) in the PEG-*b*-P(Glu) led to the formation of narrowly distributed micellar assemblies (Fig. 1) with average diameters of approximately 40 nm (Table 1). The increase in the length of the p(Glu) block slightly enlarged the diameter of DACHPt/m (Table 1). The drug content in the micelles was determined to be remarkably high in all the micelle formulations (Table 1). The [DACHPt]/[Glu] molar ratios in DACHPt/m were found to be similar for all the formulations.

3.2. Biodistribution

3.2.1. Biodistribution of free oxaliplatin and DACHPt/m prepared with PEG-b-P(Glu) 12–40

The biodistribution study was performed on CDF_1 mice ($n=6$) bearing s.c. C-26 tumors. Oxaliplatin or DACHPt/m prepared with PEG-*b*-P(Glu) 12–40 were i.v. injected. In previous studies, DACHPt/m prepared with PEG-*b*-P(Glu) 12–40 have shown remarkably prolonged blood circulation, whereas free oxaliplatin was promptly removed from circulation. The Pt in plasma was determined to be 15% of the injected dose at 24 h post-injection, and more than 8% even at 48 h after injection for DACHPt/m [22]. This prolonged blood circulation of DACHPt/m was reasonably associated with the high kinetic stability of the micelles in phosphate buffered saline at 37 °C [22].

The accumulations of oxaliplatin and DACHPt/m in normal tissues (kidney, liver, spleen, and muscle) and solid tumor (C-26 cells) are shown in Fig. 2. Oxaliplatin was rapidly distributed to each organ in agreement with its rapid plasma clearance. In contrast, DACHPt/m showed cumulative accumulation in each organ and solid tumor ($p<0.001$) due to its remarkably prolonged blood circulation time, and the Pt level in the liver, spleen, and tumor continuously increased up to approximately 48 h after injection (Fig. 2). Consequently, the DACHPt/m exhibited 20-, 4-, and 25-fold higher accumulation in the liver, spleen, and tumor, respectively, than oxaliplatin at 48 h after injection. To assess the selectivity to the solid tumor, the

Fig. 5. Antitumor activity of DACHPt-loaded micelle (DACHPt/m) prepared with PEG-*b*-P(Glu) 12–20 against s.c. C-26 tumor model ($n=6$). Saline(×); oxaliplatin at 10 mg/kg(○); 6 mg/kg(△); 4 mg/kg(◇); 2 mg/kg(□). DACHPt-loaded micelle (DACHPt/m) 12–20 at 6 mg/kg(▲); 4 mg/kg(◆); 2 mg/kg(■). A. Tumor volume (mm^3) for oxaliplatin treatment; B. Relative body weight of mice for oxaliplatin treatment; C. Tumor volume (mm^3) for DACHPt/m treatment; D. Relative body weight of mice for DACHPt/m treatment. Data are expressed as averages±S.D. *Toxic death. **$p<0.01$. ***$p<0.005$.

accumulation ratios and area under the Pt concentration-time curve (AUC) ratios of the tumor to normal tissues at 48 h after injection are summarized in Table 2. The area under the Pt concentration-time curve was calculated based on the trapezoidal rule up to 48 h. As shown in Table 2, the tumor to kidney, liver and spleen ratios were lower than 1 for oxaliplatin, suggesting no selectivity to the tumor. In contrast, the DACHPt/m exhibited accumulation and AUC ratios higher than 1.0, suggesting its selective accumulation in the tumor.

3.2.2. *Effect of P(Glu) block length on the biodistribution of micelles*

The biodistribution of the micelles prepared from PEG-*b*-P(Glu) with different p(Glu) block units in tumor-bearing mice was examined and is shown in Fig. 3. The Pt accumulation levels were studied at 24 and 48 h. All the DACHPt/m formulations showed elevated Pt levels at the tumor (Fig. 3A and B). Importantly, the amount of Pt in liver was directly correlated with the length of the p(Glu) block forming DACHPt/m. The tumor targeting efficiency of the micelles was estimated by calculating the ratio of the accumulated dose in the tumor site against the accumulated dose in the organs (Fig. 3C and D). From these results, DACHPt delivery to the tumor site by a micellar carrier seems to be extremely efficient, since all the micelles showed higher tumor/organ accumulation ratios. This efficiency was maximized for the PEG-*b*-P(Glu) 12–20-micelle formulation showing the lowest non-specific accumulation in normal tissues, thus achieving the highest relative tumor targeting. Such enhanced tumor targeting will permit expanding the therapeutic window of the micelle.

3.3. *Antitumor activity*

To evaluate the antitumor activity of DACHPt/m, CDF1 mice ($n=6$) bearing subcutaneous C-26 cells were treated i.v. four times at 2-day intervals with oxaliplatin at doses of 2, 4, 6, and 10 mg/kg or DACHPt/m (prepared with PEG-*b*-P(Glu) 12–40 and 12–20) at doses of 2, 4, and 6 mg/kg on a Pt basis. Each drug was intravenously injected on days 7, 9, 11, and 13 after inoculation, and the tumor volume after the treatment by oxaliplatin or DACHPt/m with PEG-*b*-P(Glu) 12–40 and 12–20 is shown in Figs. 4 and 5 (A and C), respectively. The relative body weight after the treatment was also monitored and shown in Figs. 4 and 5 (B and D).

The mice treated with 10 mg/kg of oxaliplatin showed toxic death after the fourth injection. Although animals treated with lower oxaliplatin doses did not show significant body weight loss, no inhibition of the tumor growth rate was observed ($p>0.05$). In contrast, the mice treated with 2 mg/kg of DACHPt/m prepared with PEG-*b*-P(Glu) 12–40 achieved significant reduction in the tumor growth rate ($p<0.001$ at day 14) without showing any body weight loss (Fig. 4C and D). Even higher tumor growth inhibition was observed for the mice treated with 4 mg/kg of PEG-*b*-P(Glu) 12–40 DACHPt/m

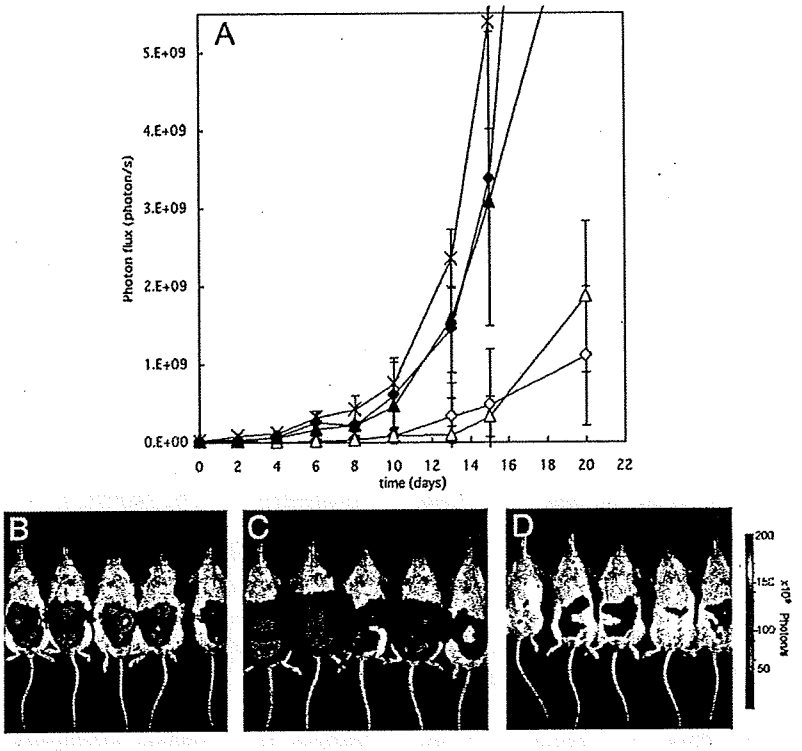

Fig. 6. Antitumor activity of DACHPt-loaded micelle (DACHPt/m) prepared with PEG-*b*-P(Glu) 12–20 against i.p. HeLa-Luc metastases ($n=5$). A. Relative photon flux from intraperitoneal metastatic sites of HeLa-luc *in vivo* treated with oxaliplatin or DACHPt-loaded micelle (DACHPt/m): Saline(×); oxaliplatin at 6 mg/kg(▲); 4 mg/kg(◆); DACHPt/m 12–20 at 6 mg/kg(△); 4 mg/kg(◇). Data are expressed as averages±S.D. *In vivo* bioluminescent images from HeLa-Luc i.p metastases at day 15: B. Saline; C. oxaliplatin 6 mg/kg; D. DACHPt/m 12–20 at 6 mg/kg.

($p<0.001$ at day 14); however, the 20% body weight loss after fourth injection suggests toxicity intensification. Increasing the DACHPt/m dose to 6 mg/kg resulted in 4 toxic deaths at day 8. The PEG-*b*-P(Glu) 12–20 micelle formulation reduced the toxicity while retaining the antitumor activity of the micelle (Fig. 5C and D). At 2 mg/kg or 4 mg/kg, this micelle formulation showed improved antitumor effect ($p<0.05$ at day 15 for 2 mg/kg; $p<0.01$ at day 15 for 4 mg/kg) compared with oxaliplatin without showing any body weight loss. At 6 mg/kg, the best tumor growth rate reduction was achieved ($p<0.005$ at day 15). The highest dose of this formulation in this experiment did not reach the lethal dose. Thus, PEG-*b*-P(Glu) 12–20 formulation for DACHPt/m seems to radically reduce drug toxicity with maintaining its potent antitumor effect, thus enlarging the therapeutic window. In addition, toxic death with DACHPt/m appeared at lower drug equivalent concentration than with oxaliplatin mainly due to the extremely high plasma AUC of DACHPt/m [22], but also because oxaliplatin is a prodrug of DACHPt. Thus, even though the drug equivalent of DACHPt/m to induce toxic death should be compared with DACHPt, it is very difficult to administer DACHPt alone due to its poor solubility.

Since DACHPt/m prepared with PEG-P(Glu) 12–70 showed higher accumulation to the liver and spleen than DACHPt/m prepared from PEG-P(Glu) 12–20 and 12–40, it will probably not increase the efficiency of the carrier. Therefore, its antitumor activity was not tested.

3.4. Antitumor activity in a bioluminescent intraperitoneal metastasis model

To evaluate the *in vivo* antitumor effect of DACHPt/m on multiple metastases generated from i.p inoculated Hela-Luc cells, SCID mice ($n=5$) were treated with free oxaliplatin or DACHPt/m beginning on day 4 post-injection. Mice with images indicating a successful i.p. inoculation on day 0 and showing *in vivo* evidence of metastasis by day 4 were placed in the drug treatment group. Free oxaliplatin or DACHPt/m were administered i.v a total of three times on day 0, 2, and 4. To quantify the bioluminescent data from metastasis, the photons emitted from the ROI in the whole animal (ventral images) were measured. The mean total photons/s were calculated from all mice. The *in vivo* bioluminescent data indicated that there was a 10-to 50-fold drop in the signal after DACHPt/m treatment (Fig. 6A). Images taken on day 15 (Fig. 6B, C, and D) indicated that DACHPt/m reduced tumor spreading in the peritoneal cavity, showing their strong growth inhibitory effect against the metastatic tumors.

4. Discussion

DACHPt/m were designed to have an extended blood circulation and a selective and high accumulation at the tumor site by the EPR effect. The average diameter of 40 nm and the hydrophilic PEG shell surrounding the micelle core are determinant features of DACHPt/m to avoid the uptake by the RES. Moreover, the sub-100 nm size of micellar nanocarriers might be optimal to achieve a remarkably high tumor extravasation efficiency and deep tumor penetration regardless of the tumor type [26]. The pharmacokinetic parameters of polymeric micelles are significantly modulated by the copolymer architecture. In this regard, the length of the micelle core-forming block not only determines the drug loading capacity of the micelle but also contributes largely to the physicochemical properties of the micelles, whereas PEG length and PEG surface density of micelles have been strongly associated with their long-circulating properties [27,28]. In this study, we prepared DACHPt/m using PEG-*b*-P(Glu) bearing different lengths of p (Glu) chain. We found that this variation considerably influences the biodistribution of micelles and thereby their antitumor activity as well as the final therapeutic window.

Drug dosage in chemotherapy is decided in part based on the competing goals of maximizing the death of malignant cells while minimizing damage to healthy cells. In the case of oxaliplatin, the major and most frequent dose-limiting toxicity observed in clinical trials was neurotoxicity [1]. Toxicological studies performed on rats with cisplatin and oxaliplatin demonstrated that the main target of neurotoxicity was the dorsal root ganglion (DRG) [29]. Although cisplatin accumulated in the DRG at a higher extent than oxaliplatin, the latter displayed more morphometric changes to the DRG after an 8-week recovery period, and this was correlated with a greater retention of oxaliplatin by the DRG in comparison with cisplatin. In contrast, neurotoxic studies revealed that CDDP-loaded micelles did not show any neurotoxicity or neuronal degeneration in rats [21]. This result might be attributed to the marked restriction of platinum accumulation into nervous tissue for the CDDP-loaded micelle, owing to the micelle size and its hydrophilic surface. Since CDDP-loaded micelles and DACHPt/m showed comparable prolonged blood circulation, preferential tumor targeting, and low accumulation in organs (Fig. 2) [20], similar reduction in the platinum accumulation at nervous tissue should be expected for DACHPt/m. Moreover, it has also been suggested that the oxalate group on oxaliplatin might immobilize calcium ions, thereby altering the amplitude of voltage-gated sodium channels of neurons [30]. The absence of an oxalate group in the DACHPt/m formulations eliminates this kind of neuronal damage.

The use of oxaliplatin is also associated with the development of severe sinusoidal injury, an aspect that had not been considered in the earlier clinical trials of oxaliplatin [31,32]. In this regard, the CDDP-loaded micelle prepared with PEG-*b*-P(Glu) 12–40 has shown transient hepatic dysfunction in rats directly related to accumulation of the micelle in liver [21]. In the present study, DACHPt/m prepared with PEG-*b*-P(Glu) 12–40 showed biphasic behavior in liver accumulation, and the Pt level in the liver remarkably increased after 8 h post-injection (Fig. 2B). Thus, the avoidance of liver uptake would be critical for the development of a clinically effective DACHPt/m formulation. We previously reported that the CDDP-loaded micelles also showed rapid accumulation of the micelle in the liver due to the morphological changes of the micelle accompanied by the release of CDDP during circulation [20]. However, such liver accumulation of the CDDP-loaded micelles was reduced for the micelle formulation from PEG-*b*-P(Glu) with a longer PEG segment [20]. Thus, the

coverage of the nanoparticles with PEG palisades is likely to be a crucial factor in the reduced liver accumulation. In this study, we evaluated the effects of the P(Glu) lengths of PEG-*b*-P(Glu) on the accumulation of the micelles in normal tissues and tumors. As a result, the micelles prepared with PEG-*b*-P(Glu) 12–20 showed considerably reduced accumulation in the liver (Fig. 3), resulting in critically reduced toxicity and, in particular, permitted a dosage increase (Fig. 5). Possibly, the use of PEG-*b*-P(Glu) with shorter P(Glu) segments may allow the formation of DACHPt/m with effective surface coverage by PEG probably due to reduced micellar core size, leading to reduction of the liver accumulation of the micelles.

DACHPt/m, prepared with PEG-b-P(Glu) 12–40 or 12–20, presented a remarkable, statistically relevant *in vivo* antitumor activity (Figs. 4 and 5), whereas free oxaliplatin failed to suppress tumor growth. The improved performance of DACHPt/m could be attributed to several aspects. The most distinguishable one is the high and preferential accumulation of DACHPt/m in the tumor due to the prolonged circulation of micelles in the bloodstream as well as the aforementioned EPR effect. In this study, DACHPt/m showed 10 times higher tumor accumulation than free oxaliplatin after 24-h post-injection, and such accumulation was maintained for an extended period (Figs. 2 and 3). On the other hand, free oxaliplatin was rapidly cleared from the bloodstream and the drug level at the tumor site was particularly low (Fig. 2). This accumulation level may be lower than the minimal amount needed to attain an efficient *in vivo* antitumor activity.

The avoidance of permanent drug inactivation by protein binding through the complexation of the platinum to the carboxylic groups in the micelle core could also be responsible for the improved biological performance of DACHPt/m over oxaliplatin. It was previously reported that, immediately after a 1 h infusion of oxaliplatin, approximately 5–30% of the drug is unbound, 10–30% is protein-bound, and 40% form complexes with hemoglobin and small molecular weight compounds in erythrocytes. Three hours later, no oxaliplatin is detectable in the plasma ultrafiltrate and only 10% is detectable in urine [33,34]. Furthermore, as many as 17 biotransformation products of oxaliplatin have been described (conjugation with methionine, cysteine, glutathione, and other low molecular weight species), but only the minor complexes $DACHPtCl_2$, $[DACHPt(H_2O)Cl]^+$ and $[DACHPt(H_2O)_2]^{2+}$ retain the ability to bind to DNA to exert the cytotoxic activity [35,36]. Among them, the dihydroxy product of oxaliplatin has been shown to have significantly greater cellular uptake and cytotoxic properties than its parent compound [37]. However, it represents a very small amount of the total plasma platinum pool after oxaliplatin administration, and therefore might not be a determinant for oxaliplatin cytotoxicity. Moreover, the formation process of $[DACHPt(H_2O)_2]^{2+}$ involves the formation of a reversible intermediate, oxalato monodentate compound, and the dissociation constant for the ring-opening step is below physiological pH (pKa=7.16). This implies that at physiological pH, the reaction favors the deprotonation of the open-ring form and the subsequent formation of the dihydroxy complex, whereas under the acidic conditions of solid tumors, ring-closure is favored and the rapid formation of oxaliplatin would be expected [38]. For DACHPt/m, the biotransformation products might be considerably different from those of oxaliplatin, and probably affect the *in vivo* performance of the drug. Since the discharge of DACHPt products from the micelle core occurs only after cleavage of the polymer-metal complex by chloride ions, and this release is enhanced at low pH, DACHPt/m probably set up conditions that favor the formation of active complexes of oxaliplatin, including the highly active $[DACHPt(H_2O)_2]^{2+}$, leading to an improved efficacy of the drug. Moreover, selective intracellular release of DACHPt complexes might occur after internalization of the micelles by endocytosis in cancer cells. As a result, DACHPt complexes may avoid extracellular inactivation and may readily induced intracellular damage.

Since systemic chemotherapy is not regarded as curative in patients with metastatic tumors and all the established therapies show low efficiency at the late stage of the disease, the antitumor activity of DACHPt/m against an i.p. metastatic tumor model was evaluated to test the potential use of micelles as a therapeutic strategy. Monitoring the development of metastatic disease is currently possible *in vivo* with the use of small animal imaging technologies including bioluminescent imaging. The results demonstrate that free oxaliplatin failed to suppress HeLa-Luc metastatic growth at any dose, whereas DACHPt/m showed a high antitumor activity while controlling tumor dissemination in the peritoneal cavity. This marked difference could be correlated to the extended blood circulation and preferential tumor accumulation of DACHPt/m, although further experiments are necessary to determine the effect of the metastatic disposition on the efficiency of the micelle. The present results revealed that DACHPt/m has a high level of antitumor activity not only on primary solid tumors but also against metastatic tumors, suggesting that DACHPt/m could be an outstanding drug delivery system for metastasis treatment.

In conclusion, we have demonstrated that decreasing the length of the core-forming block of DACHPt/m augmented their tumor specificity and drastically diminished their toxicity. Moreover, the high and preferential accumulation of the micelles at the tumor site resulted in considerable antitumor activity of DACHPt/m against primary and metastatic tumor models. Thus, DACHPt/m might be an exceptional drug delivery system for oxaliplatin active complexes.

Acknowledgments

This research was supported by a Grant-in-Aid for Scientific Research from Ministry of Education, Culture, Sports, Science and Technology of Japan as well as by the Project on the Materials Development for Innovative Nano-Drug Delivery Systems from the Ministry of Education, Culture, Sports, Science and Technology (MEXT), Japan.

References

[1] A. Ibrahim, S. Hirschfeld, M.H. Cohen, D.J. Griebel, G.A. Williams, R. Pazdur, FDA drug approval summaries: oxaliplatin, Oncologist 9 (2004) 8–12.

[2] J.M. Extra, M. Espie, F. Calvo, Phase I study of oxaliplatin in patients with advanced cancer, Cancer Chemother. Pharmacol. 25 (1990) 299–303.

[3] G. Mathé, Y. Kidani, M. Segiguchi, M. Eriguchi, G. Fredj, G. Peytavin, J.L. Misset, S. Brienza, F. de Vassals, E. Chenu, C. Bourut, Oxalato-platinum or l-OHP, a third generation platinum complex: an experimental and clinical appraisal and preliminary comparison with cis-platinum and carboplatinum, Biomed. Pharmacother. 43 (1989) 237–250.
[4] Y. Matsumura, H. Maeda, A new concept for macromolecular therapeutics in cancer chemotherapy: mechanism of tumoritropic accumulation of proteins and the antitumor agent SMANCS, Cancer Res. 46 (1986) 6387–6392.
[5] M. Yatvin, H. Miihlensiepen, W. Porschen, L. Feinendegen, J. Weinstein, Selective delivery of liposome-associated cis-dichloro-diammine platinum (II) by heat and its influence on tumor drug uptake and growth, Cancer Res. 41 (1981) 1602–1607.
[6] R. Perez-Soler, Liposomes as carriers of antitumor agents: toward a clinical reality, Cancer Treatment Rev. 16 (1989) 67–82.
[7] R. Perez-Soler, I. Han, S. Al-Baker, A.R. Khokhar, Lipophilic platinum complexes entrapped in liposomes: improved stability and preserved antitumor activity with complexes containing linear alkyl carboxylate leaving groups, Cancer Chemother. 33 (1994) 378–384.
[8] D. Avichechter, B. Schechter, R. Arnon, Functional polymers in drug delivery: carrier-supported CDDP (cis-platin) complexes carboxylates — effect on human ovarian carcinoma, React. Funct. Polym. 36 (1998) 59–69.
[9] B. Schechner, A. Newman, M. Wilnek, R. Arnon, Soluble polymers as carriers of cis-platinum, J. Control. Release 39 (1989) 75–87.
[10] X. Lin, Q. Zhang, J.R. Rice, D.R. Stewart, D.P. Nowotnik, S.B. Howell, Improved targeting of platinum chemotherapeutics. The antitumour activity of the HPMA copolymer platinum agent AP5280 in murine tumour models, Eur J Cancer. 40 (2004) 291–297.
[11] J.R. Rice, J.L. Gerberich, D. Nowotnik, S.B. Howell, Preclinical efficacy of AP5346, a novel diaminocyclohexane-platinum tumor-targeting drug delivery system, Clin. Cancer Res. 12 (2006) 2248–2254.
[12] K. Kataoka, G.S. Kwon, M. Yokoyama, Y. Sakurai, T. Okano, Block copolymer micelles as vehicles for drug delivery, J. Control. Release 24 (1993) 119–132.
[13] C. Allen, D. Mysinger, A. Eisenberg, Nano-engineering block copolymer aggregates for drug delivery, Colloids Surf., B Biointerfaces 16 (1999) 3–27.
[14] N. Nishiyama, K. Kataoka, Nano-structured devices based on block copolymer assemblies for drug delivery: designing structures for enhanced drug function, Adv. Polym. Sci. 193 (2006) 67–101.
[15] H.M. Aliabadi, A. Lavasanifar, Polymeric micelles for drug delivery, Expert Opin. Drug Deliv. 3 (2006) 139–161.
[16] N. Nishiyama, M. Yokoyama, T. Aoyagi, T. Okano, Y. Sakurai, K. Kataoka, Preparation and characterization of self-assembled polymer-metal complex micelle from cis-dichlorodiammineplatinum(II) and poly(ethylene glycol)-poly(a,b-aspartic acid) block copolymer in an aqueous medium, Langmuir 15 (1999) 377–383.
[17] N. Nishiyama, K. Kataoka, Preparation and characterization of size-controlled polymeric micelle containing cis-dichlorodiammineplatinum(II) in the core, J Control. Release 74 (2001) 83–94.
[18] N. Nishiyama, Y. Kato, Y. Sugiyama, K. Kataoka, Cisplatin-loaded polymer-metal complex micelle with time-modulated decaying property as a novel drug delivery system, Pharm. Res. 18 (2001) 1035–1041.
[19] N. Nishiyama, F. Koizumi, S. Okazaki, Y. Matsumura, K. Nishio, K. Kataoka, Differential gene expression profile between PC-14 cells treated with free cisplatin and cisplatin-incorporated polymeric micelles, Bioconjug. Chem. 14 (2003) 449–457.
[20] N. Nishiyama, S. Okazaki, H. Cabral, M. Miyamoto, Y. Kato, Y. Sugiyama, K. Nishio, Y. Matsumura, K. Kataoka, Novel cisplatin-incorporated polymeric micelles can eradicate solid tumors in mice, Cancer Res. 63 (2003) 8977–8983.
[21] H. Uchino, Y. Matsumura, T. Negishi, F. Koizumi, T. Hayashi, T. Honda, N. Nishiyama, K. Kataoka, S. Naito, T. Kakizoe, Cisplatin-incorporating polymeric micelles (NC-6004) can reduce nephrotoxicity and neurotoxicity of cisplatin in rats, Br. J. Cancer 93 (2005) 678–687.
[22] H. Cabral, N. Nishiyama, S. Okazaki, H. Koyama, K. Kataoka, Preparation and biological properties of dichloro(1,2-diaminocyclohexane)platinum (II) (DACHPt)-loaded polymeric micelles, J. Control. Release 101 (2005) 223–232.
[23] T. Tashiro, Y. Kawada, Y. Sakurai, Y. Kidani, Antitumor activity of a new platinum complex: oxalato (trans-l-diaminocyclohexane) platinum (II): new experimental data, Biomed. Pharmacother. 43 (1989) 251–260.
[24] S. Oppenheimer, Cellular basis of cancer metastasis: a review of fundamentals and new advances, Acta Histochem. 108 (2006) 327–334.
[25] Cervical cancer, NIH Consens. Statement 14 (1996) 1–38.
[26] A. Lukyanov, Z. Gao, L. Mazzola, V.P. Torchilin, Polyethylene glycol-dyacyllipid micelles demonstrate increased accumulation in subcutaneous tumors in mice, Pharm. Res. 19 (2002) 1424–1429.
[27] G.S. Kwon, S. Suwa, M. Yokoyama, T. Okano, Y. Sakurai, K. Kataoka, Enhanced tumor accumulation and prolonged circulation times of micelles-forming poly(ethyleneoxide-aspartate) block copolymers-adriamycin conjugates, J. Control. Release 29 (1994) 17–23.
[28] M. Yokoyama, T. Okano, Y. Sakurai, S. Fukushima, K. Okamoto, K. Kataoka, Selective delivery of adriamycin to a solid tumor using a polymeric micelle carrier system, J. Drug Target. 7 (1999) 171–186.
[29] G. Cavaletti, G. Tredici, M.G. Petruccioli, E. Donde, P. Tredici, P. Marmiroli, C. Minoia, A. Ronchi, M. Bayssas, G. Griffon Etienne, Effects of different schedules of oxaliplatin treatment on the peripheral nervous system of the rat, Eur. J. Cancer 37 (2001) 2457–2463.
[30] F. Grolleau, L. Gamelin, M. Boisdron-Celle, B. Lapied, M. Pelhate, E. Gamelin, A possible explanation for a neurotoxic effect of the anticancer agent oxaliplatin on neuronal voltage-gated sodium channels, J. Neurophysiol. 85 (2001) 2293–2297.
[31] L. Rubbia-Brandt, V. Audard, P. Sartoretti, A.D. Roth, C. Brezault, M. Le Charpentier, B. Dousset, P. Morel, O. Soubrane, S. Chaussade, G. Mentha, B. Terris, Severe hepatic sinusoidal obstruction associated with oxaliplatin based chemotherapy in patients with metastatic colorectal cancer, Ann. Oncol. 15 (2004) 460–466.
[32] G. Tisman, D. MacDonald, N. Shindell, E. Reece, P. Patel, N. Honda, E.K. Nishimora, J. Garris, W. Shannahan, N. Chisti, J. McCarthy, S.N. Moaddeli, D. Sargent, A. Plant, Oxaliplatin toxicity masquerading as recurrent colon cancer, J. Clin. Oncol. 22 (2004) 3202–3204.
[33] J. Liu, E. Kraut, J. Bender, R. Brooks, S. Balcerzak, M. Grever, H. Stanley, S. D'Ambrosio, R. Gibson-D'Ambrosio, K.K. Chan, Pharmacokinetics of oxaliplatin (NSC266046) alone and in combination with paclitaxel in cancer patients, Cancer Chemother. Pharmacol. 49 (2002) 367–374.
[34] C. Massari, S. Brienza, M. Rotarski, J. Gastiaburu, J.-L. Misset, D. Cupissol, E. Alafaci, H. Dutertre-Catella, G. Bastian, Pharmacokinetics of oxaliplatin in patients with normal versus impaired renal function, Cancer Chemother. Pharmacol. 45 (2000) 157–164.
[35] F.R. Luo, S.D. Wyrick, S.G. Chaney, Biotransformations of oxaliplatin in rat blood *in vitro*, J. Biochem. Molec. Toxicol. 13 (1999) 159–169.
[36] F.R. Luo, T.-Y. Yen, S.D. Wyrick, S.G. Chaney, High-performance liquid chromatographic separation of the biotransformation products of oxaliplatin, J. Chromatogr., B 724 (1999) 345–356.
[37] F.R. Luo, S.D. Wyrick, S.G. Chaney, Cytotoxicity, cellular uptake and cellular biotransformations of oxaliplatin in human colon carcinoma cells, Oncol. Res. 10 (1998) 595–603.
[38] E. Jerremalm, P. Videhult, G. Alvelius, W.J. Griffiths, T. Bergman, S. Eksborg, H. Ehrsson, Alkaline hydrolysis of oxaliplatin — isolation and identification of the oxalato monodentate intermediate, J. Pharm. Sci. 91 (2002) 2116–2121.

In Vivo Antitumor Activity of the Folate-Conjugated pH-Sensitive Polymeric Micelle Selectively Releasing Adriamycin in the Intracellular Acidic Compartments

Younsoo Bae,[†,‡] Nobuhiro Nishiyama,[†,‡] and Kazunori Kataoka*[,†,‡,§]

Center for Disease Biology and Integrative Medicine, Graduate School of Medicine, The University of Tokyo, 7-3-1 Hongo, Bunkyo-ku, Tokyo 113-0033, Japan, and Center for NanoBio Integration and Department of Materials Engineering, The University of Tokyo, 7-3-1 Hongo, Bunkyo-ku, Tokyo 113-8656, Japan. Received December 26, 2006; Revised Manuscript Received March 2, 2007

Cancer treatment efficacy and safety of the environmentally sensitive polymeric micelle drug carriers were significantly increased by optimizing the number of ligands on their surface. These micelles were designed to target the cancerous tumors through the interaction between folate and its receptors that overexpress on the cancer cell membrane while achieving pH-controlled drug release in the intracellular acidic compartments such as endosomes and lysosomes. In order to elucidate the effects of folate on cytotoxicity, biodistribution, anticancer activity, and pharmacological properties, folate concentration on the surface of the micelles was controlled by precise synthesis of two different amphiphilic block copolymers that self-assemble into spherical micelles, folate–poly(ethylene glycol)–poly(aspartate-hydrazone-adriamycin) with γ-carboxylic acid activated folate and methoxy-poly(ethylene glycol)–poly(aspartate-hydrazone-adriamycin) without folate. It is of significance that, although folate conjugation induced an extremely small change in tumor accumulation of the micelles, folate-conjugated micelles showed lower in vivo toxicity and higher antitumor activity over a broad range of the dosage from 7.50 to 26.21 mg/kg, which was 5-fold broader than free drugs.

INTRODUCTION

Precise control of the amount and uniform distribution of ligands on nanoparticles is one of the most challenging assignments in the design of polymeric drug carriers for successful active drug targeting (*1*–*3*). Indeed, a large number of studies have shown that active drug targeting is promising for effective cancer treatment (*4*–*7*). However, the questions about how many ligands are necessary for achieving efficient active drug targeting of the polymeric drug carriers are still controversial and remain to be elucidated further. In particular, when such drug carriers are tailored to deliver anticancer drugs to cancer cells systemically, it is of significant importance to confirm whether the ligand conjugation maintains their pharmacokinetic properties without decreasing antitumor activity. It is because anticancer drugs are normally highly toxic, inducing serious side effects, and although ligands can increase the interaction between the drug carriers and targeted cells in the body, they might also induce an increase in the cellular interaction with nontargeted cells, that we are not willing to deliver drugs. In order to answer these questions, we have to prepare first a drug carrier with optimal amounts of ligands, whose chemical and biological properties are fairly well established and then ascertain whether ligand installation induces any change in its biological properties.

The rationales for tumor-specific drug delivery with polymers have been reported during the past decades and are based on the characteristics of tumor tissues such as disordered and leaky vasculatures, a thick extracellular matrix, and other microenvironmental peculiarities including the hypoxic environment, expression of cancer-specific receptors, and excessive secretion of cytokines (*8*–*9*). One of the widely accepted methodologies for polymeric drug delivery is to target leaky tumor vessels and the poorly developed lymphatic drainage in the tumor tissues so that polymers and their drug conjugates can pass the tumor blood vessel wall and then accumulate in tumor tissue for a prolonged time. This methodology is explained as the enhanced permeability and retention (EPR) effect, providing the most probable theory for passive drug targeting (*10*). Nevertheless, recent studies have revealed that tumor-targeting drug delivery cannot be completely achieved only by the EPR effect because polymeric drug carriers often encounter difficulties in accessing cancer cells in the deeper place of the tumor tissues or in interacting with the targeted cells after accumulation (*11*, *12*). Polymeric drug carriers are normally required to have biocompatibility and high molecular weight to prevent protein adsorption that induces recognition by the body defense system and to increase the tumor accumulation via the EPR effect, respectively. However, these efforts frequently result in low cellular uptake of polymeric drug carriers after extravasation, reducing the actual drug concentration within the tumor due to the stagnation around the tumor tissue. As a result, we should inject polymeric drug carriers with a higher amount compared to free drugs to deliver a sufficient amount of drugs to the tumor. This is also the reason the current polymeric drug delivery systems urgently need to improve their targeting efficiency. From these aspects, active targeting has been believed to clear the problems by facilitating polymeric drug delivery systems (*13*). Active targeting can be achieved by installing ligands to the polymers or polymer assemblies so that they can interact with receptors that express on the targeted sites such as cancer cell membranes. Nevertheless, it is obvious that active targeting

* To whom correspondence should be addressed: Kazunori Kataoka, Ph.D. Professor, Department of Materials Engineering, Graduate School of Engineering, The University of Tokyo, 7-3-1 Hongo, Bunkyo-ku, Tokyo 113-8656, Japan. Phone +81-3-5841-7138, Fax +81-3-5841-7139, E-mail: kataoka@bmw.t.u-tokyo.ac.jp.

† Graduate School of Medicine.

‡ Center for NanoBio Integration.

§ Department of Materials Engineering.

10.1021/bc060401p CCC: $37.00
Published on Web 05/09/2007

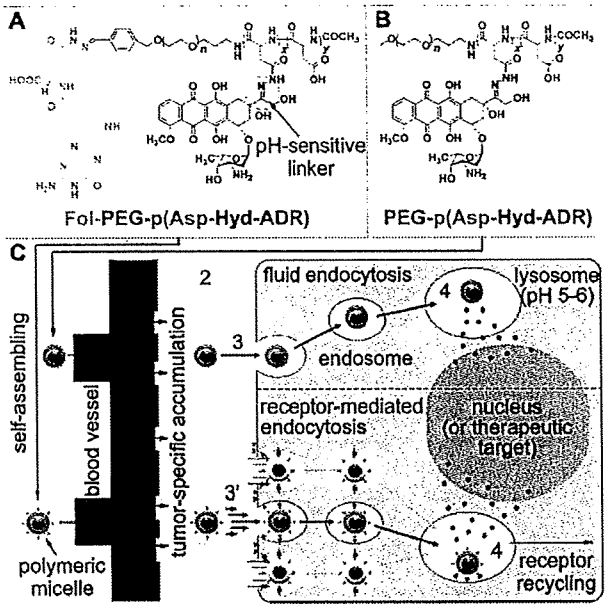

Figure 1. Design of polymeric micelles and the rationale for active drug delivery. Chemical structures of folate–poly(ethylene glycol)–poly(aspartate-hydrazone-adriamycin) and methoxy-poly(ethylene glycol)–poly(aspartate-hydrazone-adriamycin) block copolymers (A and B). As shown in panel C, these polymers can self-assemble into the polymeric micelles that can effectively achieve systemic drug delivery and tumor-specific accumulation (1 and 2). The micelles are then uptaken by the cancer cells via fluid endocytosis (3) or receptor-mediated endocytosis (3′) depending on surface design for accelerating endocytosis (e.g., folate conjugation). Anticancer drugs, adriamycin (ADR), that are conjugated through a pH-sensitive hydrazone bond can be released from the micelles in the acidic intracellular compartments such as endosomes or lysosomes where pH ranges from 5 to 6 (4).

cannot be achieved until passive targeting of drug carriers is successfully accomplished.

Amphiphilic block copolymers are useful tools for the preparation of supramolecular assemblies. By precisely controlling their molecular weight and the hydrophilic/hydrophobic balance, we can prepare spherical supramolecular nanoassemblies, also known as "the polymeric micelles", with a hydrophilic shell that envelopes a hydrophobic core (*14*). The polymeric micelle is considered to be one of the most successful polymeric drug carrier formulations, because it is characterized by high drug loading contents, prolonged blood circulation, and selective tumor accumulation (*15*). Most notably, their chemical, biological, and pharmacological properties have been widely studied, and thus we can easily investigate the effect of active targeting (*16, 17*). In this study, poly(ethylene glycol)–poly(β-benzyl-L-aspartate) block copolymers (PEG–PBLA) were synthesized for the basic platform for the preparation of the polymeric micelles, and these micelles were further functionalized to conjugate anticancer drugs and ligands. Figure 1 shows the chemical structures of the block copolymers used in this study. Anticancer drugs, adriamycin (ADR), were conjugated to the side chains of the core-forming poly(aspartic acid) block through a hydrazone linkage, which can be selectively cleaved under the acidic conditions with pH ranging from 5 to 6, corresponding to the intracellular vesicles such as the endosomes and lysosomes (*18*). In our previous studies, we have reported that this intracellular pH-sensitive polymeric micelle showed remarkably low toxicity and high in vivo efficacy (*19*). It was also confirmed that the pH-sensitive micelles can release drugs selectively by responding to a decrease in intracellular pH of the cell, and therefore, drug leakage from the micelles decreases during the blood circulation and tumor-specific drug delivery efficiency increases. In the meantime, folate was conjugated at the end of the shell-forming poly(ethylene glycol) (PEG) block for active targeting. Folate, an anionic form of folic acid, is a vitamin B9 that helps the production and maintenance of new cells. Originally, folate was necessary for the restoration of the DNA damage that may induce cancer. However, interestingly, cancer cells overexpress folate-binding proteins (FBPs) on their cell membranes (*20, 21*). This is probably due to the DNA replication that is supported by folate, which is also a prerequisite for the cancer growth. More interestingly, cancer cells are believed to reduce chemotherapeutical response by regulating intracellular folate concentration (*22*). Therefore, we can actively guide polymeric drug carriers to cancer cells in the body by folate conjugation (*23*). It must be noticed that FBP binding activity of folate drastically changes depending on its activated state, which is distinguished by an inactive α- and active γ-carboxyl activated form (*24*). Herein, we conjugated folate to PEG at its γ-carboxyl position to maintain its activity by precision synthesis as reported elsewhere (*25–27*).

The objectives of this research are to ascertain whether folate conjugation can enhance antitumor efficacy of the pH-sensitive micelles without deteriorating the characteristics of the micelles as a long-circulating drug carrier with high tumor accumulation, and to determine how much folate concentration is optimum for achieving effective passive and active drug targeting simultaneously. Such information would be beneficial to the future design and preparation of ligand-installed multifunctional polymeric drug carriers for cancer treatment.

EXPERIMENTAL PROCEDURES

Materials and Devices. Acetic anhydride (AA), chloroform ($CHCl_3$), *N,N*-dimethyl formamide (DMF), dimethyl sulfoxide (DMSO), hexane, methanol (MeOH), methanesulfonyl chloride (CH_3SO_2Cl), triethylamine (TEA), trifluoroacetic acid (TFA), trifluoroacetic anhydride (TFAA), and tetrahydrofuran (THF) were purchased from Wako Pure Chemical Industries, Japan. DMF, hexane, and THF were distilled twice following standard procedures. Carbazic acid *tert*-butyl ester (CAt-BE) and potassium carbonate (K_2CO_3) were purchased from Tokyo Kasei Organic Chemicals, Japan. These chemicals were used without further purification. Daunorubicin (DAU), folic acid (Fol), 4-(diethoxymethyl)benzaldehyde, and sodium borohydride ($NaBH_4$) were purchased from Sigma Chemical, U.S.A. Ethylene oxide (EO) was from Sumitomo Seika Chemicals, Japan, and dried over calcium hydride followed by distillation. β-Benzyl-L-aspartate (BLA) was from Sigma, and α-methoxy-ω-amino-poly(ethylene glycol) (MeO-PEG-NH_2) was from Nippon Oil and Fats, Japan. PEG was purified using an ion-exchange gel column (CM-Sephadex C-50, Amersham Pharmacia Biotech, U.S.A.) prior to the synthesis of the block copolymers. Adriamycin hydrochloride (ADR) was kindly provided by Nippon Kayaku, Japan, and its purity was checked by reversed-phase liquid chromatograpy (RPLC). Sephadex LH-20 gel was from Amersham Pharmacia Biotech, Sweden. Gel permeation chromatography (GPC) analysis was carried out using a TOSOH HLC-8220 equipped with TSK-GEL columns (G4000PWXL and G3000PWXL). Internal refractive index (RI) and ultraviolet–visible absorption (UV) detectors were used. DMF containing 10 mM of LiCl was used as an eluant at a flow rate of 0.8 mL/min at 40 °C. ^1H NMR spectra were measured with a JEOL EX300 spectrometer (JEOL, Japan). Flow cytometric analysis was performed with EPICS XL Flow Cytometry Systems (Beckman Coulter, U.S.A.). The multimode reader Mithras LB 940 (Berthold Technologies, U.S.A.) was used for in vitro cytotoxicity evaluation using a CellTiter-Glo luminescent cell viability assay kit (Promega, U.S.A.).

Cell Lines and Animals. A human pharyngeal cancer cell line KB was purchased from Health Science Research Resources Bank, Japan. Cells were cultured in Dulbecco's Modified Eagle cell culture Medium (DMEM, Sigma, U.S.A.) containing 10% FBS under a humidified atmosphere with 5% CO_2 at 37 °C. CD-1 nude mice (female, 6-week-old) were purchased from Charles River, Japan. The animals were cared for and all experiments were performed in compliance with the Guide for the Care and Use of Laboratory Animals as adopted and promulgated by the National Institutes of Health. The number of independent experiments is stated as *n*, and the experimental data are expressed as mean and mean ± SEM for relative and absolute values, respectively.

Synthesis of Self-Assembling Amphiphilic Block Copolymers. In this study, we synthesized two different types of self-assembling amphiphilic block copolymers for the preparation of the micelles, folate−poly(ethylene glycol)−poly(aspartate-hydrazone-adriamycin) [Fol−PEG−p(Asp-Hyd-ADR)] and methoxy-poly(ethylene glycol)−poly(aspartate-hydrazone-adriamycin) [PEG−p(Asp-Hyd-ADR)]. Synthesis methods for these block copolymers were previously reported elsewhere (*25*). Briefly, Fol−PEG−p(Asp-Hyd-ADR) was synthesized via seven steps as follows.

a. Synthesis of Heterobifunctional α-4-(Diethoxymethyl)-benzylacetal-ω-amine-poly(ethylene glycol) (aceBz-PEG-NH_2). 4-(Diethoxymethyl)benzaldehyde (5 g) was reduced with $NaBH_4$ (1 g) in dry ethanol (100 mL). Obtained 4-(diethoxymethyl)-benzylalcohol (0.19 g) was then mixed with potassium naphthalene (115 mg) in dry THF (30 mL) to prepare potassium 4-(diethoxymethyl)benzylalkoxide, followed by the addition of distilled EO (11.9 g) for anionic polymerization to obtain aceBz-PEG-OH. After 2 days of reaction at 25 °C, CH_3SO_2Cl (0.62 g) and TEA (0.82 g) were added to aceBz-PEG-OH in 25 mL of THF to prepare an intermediate product aceBz-PEG-OSO_2CH_3, which was then mixed with ammonia solution (25%) to produce aceBz-PEG-NH_2.

b. Selective Functionalization of Folic Acid at its γ-Position of the Glutamate Residue with Hydrazide (Fol-hyd). An excess amount of TFAA (3 mL) was added dropwisely to folic acid (2 g) in THF (20 mL) to prepare N_{10}-(trifluoroacetyl)pyrofolic acid. This pyrofolic acid (500 mg) was reacted with CAt-BE (1.6 g) in 20 mL of dry DMF at 40 °C overnight. Prepared folate-hydrazide-BOC was treated with TFA to obtain Fol−Hyd.

c. Preparation of β-benzyl-L-aspartate N-Carboxy Anhydride (BLA−NCA). 5.77 g of triphosgene was added to 10 g of β-benzyl-L-aspartate in 150 mL of dry THF at 40 °C, and the reaction was allowed to proceed until the solution became clear. Prepared β-benzyl-L-aspartate *N*-carboxy anhydride (BLA−NCA) was purified by recrystallization from hexane.

d. Ring-Opening Polymerization of BLA−NCA by Using aceBz-PEG-NH_2 as a Macroinitiator to Obtain 4-(Diethoxymethyl)benzyl Acetal−poly(ethylene glycol)−poly(β-benzyl-L-aspartate) (aceBz−PEG−PBLA). 6 g of aceBz−PEG−NH_2 with molecular weight of 12 000 and 5 g of BLA−NCA were dissolved in 30 mL and 10 mL of DMSO, respectively. NCA solution was added to PEG solution at 40 °C, and the reaction was allowed to proceed for 2 days.

e. ω-Amino Group Protection for aceBz−PEG−PBLA Block Copolymers, Followed by α-Acetal Group Deprotection and Subsequent Conjugation of Fol−hyd at the End of the PEG Chain (Fol−PEG−PBLA). The ω-amino group of aceBz−PEG−PBLA was protected by AA to prevent dimerization between aldehyde−benzyl−poly(ethylene glycol)−poly(β-benzyl-L-aspartate) (CHO−Bz−PEG−PBLA) block copolymers, which can be prepared by deprotecting acetal groups of aceBz−PEG−PBLA with 0.1 N HCl aqueous solution. End-group protected CHO−Bz−PEG−PBLA (250 mg) was then mixed with Fol−Hyd (50 mg) in dry DMF to prepare Fol−PEG−PBLA.

f. Substitution Benzyl Esters at the Side Chain of Fol−PEG−PBLA with Drug-Binding Hydrazide Groups to Prepare Fol−PEG−p(Asp-Hyd). 500 mg of Fol−PEG−PBLA was dissolved in 10 mL of dry DMF, and anhydrous hydrazine (0.62 mg) was added to the solution. The reaction was allowed to proceed at 40 °C for 2 h, followed by deprotection of remained benzyl groups with 0.1 N NaOH aqueous solution at 25 °C. Polymers were dialyzed against 0.25% ammonia solution and collected by freeze-drying.

g. Conjugation of ADR at Its 13-C Carbonyl with the Hydrazide Groups of Fol−PEG−p(Asp-Hyd) through a pH-Sensitive Schiff Base Linkage. Fol−PEG−p(Asp-Hyd) (100 mg) in 50 mL of DMSO was mixed with an excess amount of ADR-HCl (100 mg) with respect to drug-binding hydrazide residues. The mixed solution was stirred at room temperature for 3 days. After precipitation from ether, Fol−PEG−p(Asp-Hyd-ADR) was redissolved in 10 mL of DMF and purified by gel filtration using a Sephadex LH-20 column. In the case of PEG−p(Asp-Hyd-ADR), MeO-PEG-NH_2 was used as a macroinitiator for BLA−NCA polymerization at step (d) instead of aceBz−PEG-NH_2, following the procedures from steps (e) to (g).

Preparation of the Folate-Conjugated pH-Sensitive Polymeric Micelles. The folate-conjugated pH-sensitive polymeric micelles were prepared from Fol−PEG−p(Asp-Hyd-ADR) alone or in combination with PEG−p(Asp-Hyd-ADR) block copolymers in various molar ratios to change folate contents (0%, 1%, 2%, 5%, 10%, 25%, 50%, and 100%). We distinguish the micelles from Fol−PEG-p(Asp-Hyd-ADR) and PEG−p(Asp-Hyd-ADR) by the notations of FMA and MA, which denote folate-conjugated micellar adriamycin and micellar adriamycin, respectively. For the preparation of FMA and MA, 250 mg of each Fol−PEG−p(Asp-Hyd-ADR) and PEG−p(Asp-Hyd-ADR) were dissolved in 5 mL of DMSO. Polymer solutions were then added dropwise into 95 mL of Tris−HCl buffer solution (10 mM, pH 7.4), sonicated at 25 °C for 10 min, and diluted further with 900 mL of Tris−HCl buffer. The polymer solutions were concentrated by Amicon Ultra-15 Centrifugal Filter Units (Millipore, U.S.A.) with molecular weight cutoff (MWCO) 30 000 kDa. 12 mL of the solutions in each swinging bucket rotor were spun at 1500 *g* at 25 °C for 15 min. During repetitive centrifugation, additional Tris−HCl buffer was added to the solutions until DMSO was completely removed. Concentrated micelle solutions were filter-sterilized and stored in aliquots at 4 °C for future use. Drug concentration was determined by UV at 490 nm, based on the calibration curve of free ADR.

Table 1. Polymer Compositions

compound	composition[a]	polydispersity index[d] (Mw/Mn)	drug loading content (wt %)
PEG-PBLA	12−42[b]	1.12	
Fol-PEG-PBLA	12−40[b]	1.14	
PEG-p(Asp-Hyd-ADR)	12−42−33−15[c]		33.84
Fol-PEG-p(Asp-Hyd-ADR)	12−40−34−14[c]		34.32

[a] The compositions of the block copolymers are abbreviated *X*−*Y* and *X*−*Y*−*Z*−*A*. The letter *X* stands for molecular weight × 10^{-3} of poly(ethylene glycol), while *Y*, *Z*, and *A* denote the numbers of aspartic acid, hydrazide, and adriamycin (ADR), respectively. [b] The values were calculated from the peak area ratio determined by ^{1}H NMR between poly(ethylene glycol) and benzyl groups of the PBLA block. [c] The numbers of hydrazide groups and ADR were determined by ^{1}H NMR and reversed-phase liquid chromatography (RPLC), respectively. [d] Polydispersity was measured for PEG−PBLA and Fol−PEG−PBLA to ensure the purity of starting materials.

Table 2. Particle Size and ζ Potential of the Micelles with Varying Folate Contents

	folate conjugation[a] (%)							
	0 (MA)	1 (FMA1)	2 (FMA2)	5 (FMA5)	10 (FMA10)	25 (FMA25)	50 (FMA50)	100 (FMA100)
particle size[b] (nm)	64.21	65.34	63.79	68.35	69.22	72.51	77.47	91.29
polydispersity index (μ/Γ^2)	0.1018	0.0951	0.1096	0.1232	0.1318	0.1437	0.1661	0.1973
ζ potential (mV)	−0.39	0.11	−0.67	−1.07	−1.98	−2.33	−6.95	−9.25

[a] It was determined by the mixing ratio of folate-conjugated block copolymers to the block copolymers without folate conjugation. [b] The micelles were filter-sterilized using 0.45 μm filter units (Millex-HV, Millipore, Co., Ltd., U.S.A.) prior to the measurements.

In Vitro Cytotoxicity Assay. In order to determine in vitro cytotoxicity of the micelles, a human pharyngeal cancer cell line KB was incubated with FMA, MA, and free ADR in various concentrations, changing exposure time. Exponentially growing KB cells were seeded on a 96-well culture plate (2000 cells/well) and preincubated for 24 h, followed by coincubation with the samples. After 3 and 24 h, cell culture media were replaced with fresh media, and the cells were incubated further for additional 24 h. The number of viable cells was determined by CellTiter-Glo luminescent cell viability assay ($n = 8$) that provides a convenient, rapid, and sensitive procedure based on quantitation of ATP, which signals the presence of metabolically active cells (*28*).

Flow Cytometric (FCM) Analysis. Cellular uptake of the micelles was analyzed by an EPICS XL Flow Cytometry Systems (Beckman Coulter, U.S.A.) monitoring autofluorescence of ADR accumulated in the cell. KB cells were seeded on a 12-well culture plate (30 000 cells/well) and preincubated for 24 h, followed by coincubation with FMA, MA, and ADR (10 mg/mL) for 3 and 24 h. The cells were then washed three times with PBS, detached by trypsinization, spun down by centrifugation, and dispersed again in PBS for FCM analysis. Data were acquired and processed with the accompanying software (*EXPO 32*).

Surface Plasmon Resonance (SPR) Analysis. Interaction between FBP and the micelles was analyzed by surface plasmon resonance (SPR) measurements using BIAcore 3000 (Biacore, Sweden). FBP was immobilized on the surface of a sensor chip (3 ng/mm^2 of FBP per channel), following the procedures provided by the manufacturer. FBP binding effects of both FMA and MA were evaluated at a flow rate of 10 μL/min with a concentration of 200 μg/mL. The micelles were allowed to flow for 30 min, and all samples were tested by replacing sensor chips on which FBPs were newly immobilized.

Pharmacological Study. Tumor-bearing mice were prepared by transplanting KB cells on the abdominal region of CD-1 nude mice (female, 6-week-old, $n = 6$, Charles River, Japan). When the tumor volume reached 100 mm^3, the micelles and free ADR as control were intravenously injected in a volume of 0.1 mL/10 g body weight. The drug dose was 10 mg/kg for both free ADR and the micelles (ADR equivalent). After drug injection, the blood, tumor, and major organs (heart, kidney, liver, and spleen) were collected at 0.5, 1, 3, 6, 9, and 24 h, followed by HPLC analysis as previously reported (*19*). Briefly, plasma was separated from the blood, and the tissues were homogenized prior to the measurements. Daunorubicin (DAU) was added to the specimens as an internal standard in 2 μg/mL, depending on sample amount. 200 μL of 10 mM HCl solution was then added to the specimens to cleave drug conjugation, and 1 mL of 100 mM ammonia buffer (pH 9.0) was applied after 24 h incubation. 5 mL of $CHCl_3$/MeOH (2:1) mixed solution was also added to the solution, and ADR and DAU were extracted by vigorous vortexing at 25 °C for 15 min. The organic layer was collected using Pasteur pipets and evaporated at 40 °C after centrifugation (1900 *g*, 15 min, 4 °C). Dry drugs were redissolved in 100 μL of DMF and injected to RPLC equipped with a μ Bondasphere 5μ C4 300 column and a fluorescence detector (Ex 485 nm, Em 560 nm). The area under the curve of concentration (AUC) vs time was calculated by the trapezoidal rule with the time points of 0.5, 1, 3, 6, 9, and 24 h. The unit for AUC is defined as % dose/mL plasma × h or % dose/g organ × h for the blood or other tissues (tumor, kidney, liver, spleen, and heart), respectively.

Table 3. Time-Dependent Increase in Cytotoxicity and Cellular Uptake of the Micelles ($n = 8$)[a]

sample	exposure time (h)	IC_{50}[b] (μg/mL ± SD)	relative index[c]	cellular uptake[d] (%)
ADR	3	0.069 ± 0.014	1.97	100.00
	24	0.035 ± 0.011	1	100.00
FMA100	3	0.172 ± 0.017	4.91	92.51
	24	0.041 ± 0.012	1.17	94.95
MA	3	N.D.[e]	N.D.[e]	40.20
	24	0.263 ± 0.013	7.51	82.05

[a] Data were obtained from the eight independent experiments using a human pharyngeal cancer cell KB. [b] IC_{50} means the inhibitory concentration of the drugs required for reducing 50% of cell proliferation. The drug concentration of the micelles was calculated with respect to free ADR equivalents. [c] Relative index means the ratio between the IC_{50} of free ADR after 24 h incubation and the samples. [d] Cellular uptake of the micelles was analyzed by flow cytometric analysis monitoring autofluorescence of ADR accumulated in the cell. [e] N.D. means not determined.

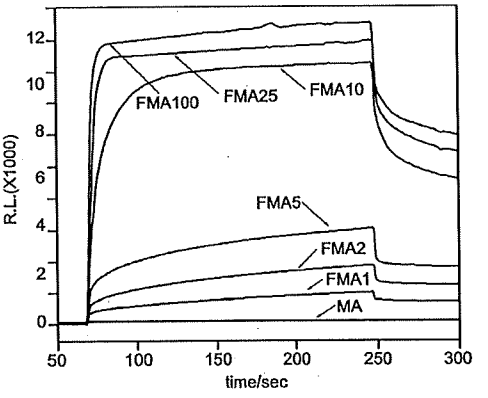

Figure 2. Surface plasmon resonance (SPR) analysis. FBP-binding selectivity of folate-conjugated micelles was evaluated by SPR measurements (eluent, 100 mM phosphate buffer; pH 7.4; flow rate, 10 mL/min; density of folate-binding protein, 3 ng/mm per channel; sample concentration, 200 μg/mL). Folate concentration on the surface of the micelles was varied to determine the optimum substitution rate.

In Vivo Antitumor Activity Evaluation. Tumor-bearing mice were prepared as described above. The micelles were injected from the tail vein three times with a four day interval in various doses (5, 10, 20, and 40 mg/kg). This administration schedule was based on the optimum regimen for free ADR as a control. However, free ADR was applied to the mice in limited doses (5, 10, and 15 mg/kg) due to the serious toxicity. Tumor growth and body weight of mice were checked at every second day. Tumor volume was calculated as volume $V = {}^1/_2 \times LW^2$, where the letters L and W denote the long and short diameters of the tumor tissue. Cancer treatment efficacy was analyzed by a treatment to control (T/C) ratio $= (V_c - V_t) \times 100/V_c$, where

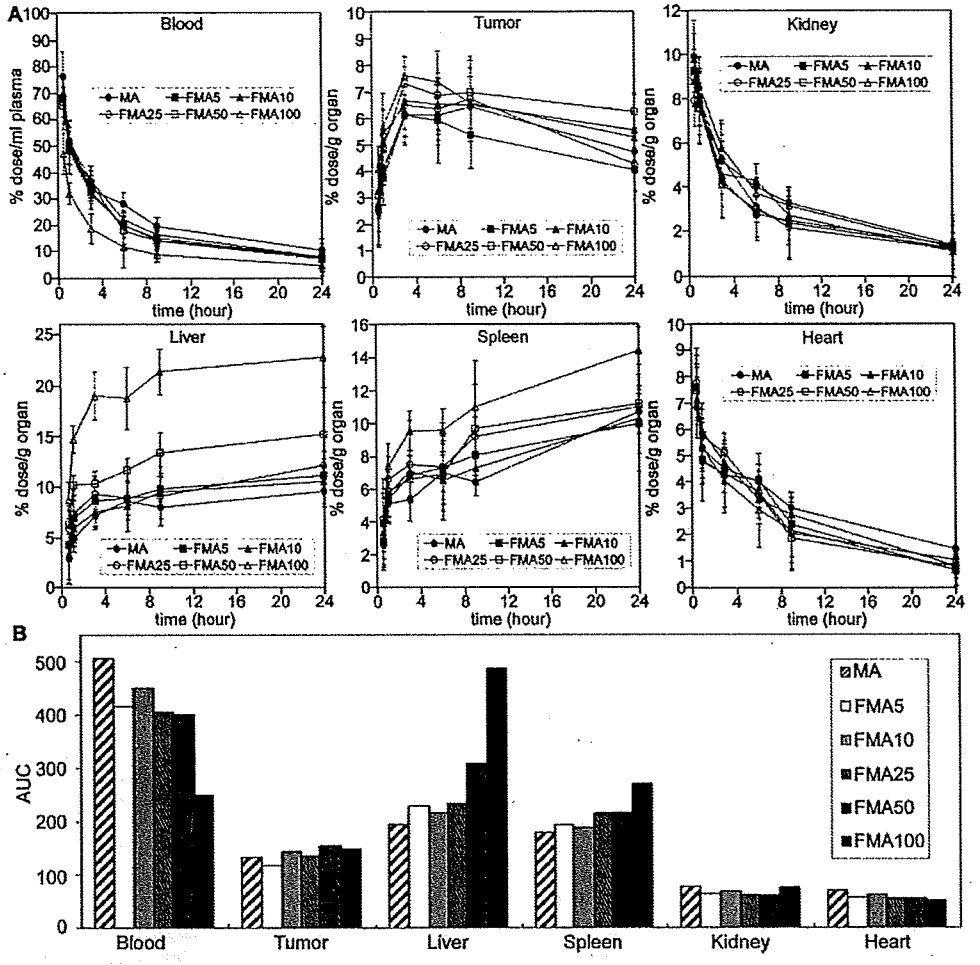

Figure 3. Pharmacokinetic profiles. Distribution of the micelles with varying folate amounts was measured in the blood compartment, tumor tissue, and major organs such as the liver, spleen, kidney, and heart (A). Experiments were carried out using tumor-bearing CD-1 nude mice (female, 6-week-old, $n = 6$) when the tumor volume reached 100 mm^3. Data are expressed as mean and mean ± SEM for relative and absolute values, respectively. Accumulation amounts for each micelle are compared in terms of the areas under the curve of concentration (AUC) vs time up to 24 h time period (B).

V_c and V_t are the mean tumor volumes of the control and the treated mice, respectively. The effective dose (ED) of each micelle was determined as the T/C ratio = 50, which means the average tumor volume of the mice decreased 50% of control values by drug treatments. The toxic dose (TD) was defined as the dose that causes 20% decrease in body weight of the mice after drug injection.

RESULTS AND DISCUSSION

Preparation of the Folate-Conjugated pH-Sensiive Polymeric Micelles (FMA). The molecular weight and composition distributions of self-assembling amphiphilic block copolymers, folate−poly(ethylene glycol)−poly(aspartate-hydrazone-adriamycin) [Fol−PEG−p(Asp-Hyd-ADR)] and α-methoxy-poly(ethylene glycol)−poly(aspartate-hydrazone-adriamycin) [PEG−p(Asp-Hyd-ADR)], were determined by GPC and ^{1}H NMR. Table 1 shows that these block copolymers were successfully prepared with a controlled number of hydrazide groups and ADR. It is noticeable that Fol−PEG−p(Asp-Hyd-ADR) block copolymers did not form any dimers or aggregates after folate conjugation. In addition, most notably, folate was functionalized only at γ-carboxylate position of its glutamate residue in this study by precision synthesis, as we previously reported elsewhere (*25*). This enables every folate molecule that is conjugated to the block copolymers to remain active, distinguishing our system from other folate conjugates. In many studies, folate molecules have been conjugated by using carbodiimide coupling reagents. The folate conjugated in this way is prone to making a mixture of α- and γ-carboxylate-functionalized forms. Because the α-carboxylate-functionalized form of folate loses its activity, the carbodiimide coupling method is substantially accompanied by the problems of undesirable introduction of inactive folate, which induces insufficient conjugation or incorrect quantification of active folate (*23, 24*). To the contrary, herein we can exclude the possibility that folate becomes inactive after conjugation, and therefore, it is able to clearly investigate the effects of folate conjugation on the biological properties of the micelles.

The particle size and ζ potential of the micelles were analyzed by Zetasizer Nano (Malvern, U.K.), and data are summarized in Table 2. Each micelle from Fol−PEG−p(Asp-Hyd-ADR) and PEG−p(Asp-Hyd-ADR) was abbreviated as FMA and MA, which denote folate micellar adriamycin and micellar adriamycin (without folate), respectively. The successive number after the abbreviated term of FMA in some descriptions indicates the mol % of Fol−PEG−p(Asp-Hyd-ADR) block copolymers in the micelles. For instance, FMA10 means that the micelles were prepared from 10% of Fol−PEG−p(Asp-Hyd-ADR) and 90% of PEG−p(Asp-Hyd-ADR) block copolymers. In all cases, the micelles exhibited particle sizes between 60 and 90 nm, while the distribution was narrow and monodisperse. Surface charge

of the micelles became negative, which is probably due to the carboxylic group remaining at the α-position of glutamate of the folate molecule. Although the micelle size slightly increased as folate concentration increased, these data demonstrate that the size and surface charge of the prepared micelles were still suitable for tumor-specific accumulation via the EPR effect after folate conjugation. When the micelle solutions were concentrated, however, aggregation between particles was observed in the case of FMA100. Such aggregation was able to be suppressed by decreasing the folate substitution ratio. Considering that MA (or FMA0) showed no aggregation during concentration, it is most probable that folate substitution increases the local concentration of folate molecules on the micelle surface, and thus, FMA aggregated due to the intermicellar hydrophobic interaction (*29*). Nevertheless, it must be noted that the micelles stably dispersed with 60−90 nm diameter up to 5 mg/mL concentration irrespective of folate substitution ratio. Because a high drug loading content (~30 wt %) is one of the characteristic advantages of the micelles, injecting the micelles above this concentration would not be realistic in terms of determining the injection dosage of ADR whose lethal dose ranges from 12.7 to 13.2 mg/kg. Therefore, it is concluded that the micelles with varying folate contents were stable at a size suitable for systemic drug delivery with sufficient drug concentration.

Folate Conjugation Significantly Increased in Vitro Cytotoxicity and Cellular Uptake of the Micelles. Table 3 shows a change in proliferation of KB cells treated by FMA100, MA, and free ADR and cellular uptake. It is of interest that the 50% inhibitory concentrations (IC_{50}) of cell growth decreased significantly in the case of the micelles by folate conjugation. Notably, cytotoxicity of FMA100 was as high as that of free ADR after 24 h incubation despite their different internalization mechanisms. In our previous studies, it is confirmed that this pH-sensitive micelle, which was designed to selectively release drugs in the intracellular region, requires relatively long exposure time sufficient for inhibiting cell growth (> 10 h). It is because the micelles are required to enter the cell first and to release drug by sensing pH so that the released drugs accumulate in cell nuclei to intercalate with DNA, inducing cell death. In comparison with MA, FMA100 showed efficient cytotoxicity with a short exposure time of 3 h. These results suggest that folate conjugation promotes the interaction between the micelles and the cell. It is generally known that KB cells overexpress folate-binding proteins (FBPs) on the cell membrane, and therefore the FBPs can take up FMA100 to the cell interior efficiently via receptor-mediated endocytosis. Such enhanced cellular uptake probably induced higher cytotoxicity of FMA100 even with short exposure time. This hypothesis was also confirmed by flow cytometric analysis. As also summarized in Table 3, cellular uptake of FMA100 increased by folate conjugation, and such an increment corresponds well with enhanced cytotoxicity. Consequently, it is confirmed that folate conjugation enhanced cytotoxicity of the micelles by increasing cellular uptake and intracellular drug concentration.

FMA Recognized Folate-Binding Proteins (FBPs) Selectively and Strongly. Although in vitro cytotoxicity assay and flow cytometric analysis have proven that high efficacy of FMA was due to the increased intracellular drug concentration, the scientific evidence that elucidates the role of folate in accelerating cellular uptake was still required. In order to confirm the interaction between FMA and folate binding proteins (FBPs), we carried out surface plasmon resonance (SPR) analysis by using a sensor chip on which FBP molecules were immobilized. It is also of great importance to verify how folate concentrations affect FBP binding properties of the micelles, so we prepared FMA with varying folate substitution rates from 100% to 0%.

Table 4. Tumor-Specific Accumulation of the Micelles

sample	blood	tumor	liver	spleen	kidney	heart
AUC[a]						
MA	506.42	132.67	194.45	179.37	76.96	69.48
FMA5	415.53	117.13	229.35	193.65	63.15	57.01
FMA10	450.38	143.60	215.97	187.98	68.45	61.79
FMA25	405.17	135.48	233.33	215.24	61.58	55.59
FMA50	400.76	155.13	308.99	216.80	60.91	54.99
FMA100	250.16	147.86	487.30	270.14	76.10	51.87
			K_b value[b]			
MA	1	0.26	0.38	0.35	0.15	0.14
FMA5	1	0.28	0.55	0.47	0.16	0.15
FMA10	1	0.32	0.48	0.42	0.16	0.15
FMA25	1	0.33	0.58	0.53	0.17	0.16
FMA50	1	0.39	0.77	0.54	0.16	0.15
FMA100	1	0.59	1.95	1.08	0.30	0.25
			tumor to organ ratio[c] (AUC_{tumor}/AUC_{organ})			
MA	–	1	0.68	0.74	1.72	1.91
FMA5	–	1	0.51	0.60	1.81	1.92
FMA10	–	1	0.66	0.76	2.04	2.12
FMA25	–	1	0.58	0.63	1.94	2.16
FMA50	–	1	0.50	0.72	2.48	2.59
FMA100	–	1	0.30	0.55	1.94	2.41

[a] AUC denotes the area under a concentration curve that is obtained from the pharmacokinetic study with time points at 0.5, 1, 3, 6, 9, and 24 h. Values were calculated on the basis of the trapezoidal rule up to 24 h after intravenous injection. The unit for AUC is defined as % dose/mL plasma × h or % dose/g organ × h for the blood or other tissues (tumor, kidney, liver, spleen, and heart), respectively. [b] K_b value is defined as $[K_b = C_{tissue}/C_{blood}]$ where C_{tissue} and C_{blood} are the drug concentrations in the tissue and the blood, respectively. Each K_b value indicates distribution of the drugs in the vascular space ($K_b < 0.1$), extracellular space ($0.1 < K_b < 0.5$), and intracellular space ($0.5 < K_b$). [c] Tumor selectivity of the micelles was determined by calculating the relative accumulated concentrations between the tumor tissues and each organ (AUC_{tumor}/AUC_{organ}).

Figure 2 shows SPR signal intensity versus time for individual micelle samples. The micelles were flowed into the sensor channel for 3 min and rinsed with fresh buffer solution. The signal change indicates that FMA binds promptly and strongly to FBP in various folate contents while MA showed no interaction with FBP. Interestingly, FMA was able to recognize FBP even with 10% folate substitution ratio. However a significant decrease was found in the FBP binding effect between FMA10 and FMA5. In the meantime, the folate substitution rates can be converted from a percent to mol wt % on the basis of the molecular weight of block copolymers and the mixing ratio. It shows that 100% folate substitution ratio corresponds to 16.9 mmol wt % for a single micelle, and FMA10 and FMA5 were calculated to contain 1.7 and 0.8 mmol % of folate molecules, respectively. Therefore, these data revealed that the micelles require only a small quantity of folate to recognize FBPs. Folate is known to have a high affinity for FBP ($K_d < 1$ nM), and such high affinity seems to provide a strong binding property of FMA (*23, 24*).

Optimum Amounts of Folate-Facilitated Tumor Targeting Properties of the Micelles with Long Blood Circulation. The information regarding the relation between the amount of folate and biodistribution of the micelles is of primary importance to determining the compositions of FMA. Such compositions should be considered to maintain the balance between passive and active tumor targeting to realize an ultimate goal of drug delivery systems. For these reasons, we have investigated the biodistribution of FMA by changing folate contents. Figure 3 shows the distribution of the micelles in the blood compartment, tumor tissues, and major organs such as the liver, spleen, kidney, and heart after the intravenous injection. The area under a concentration curve (AUC) shows that the micelles circulated

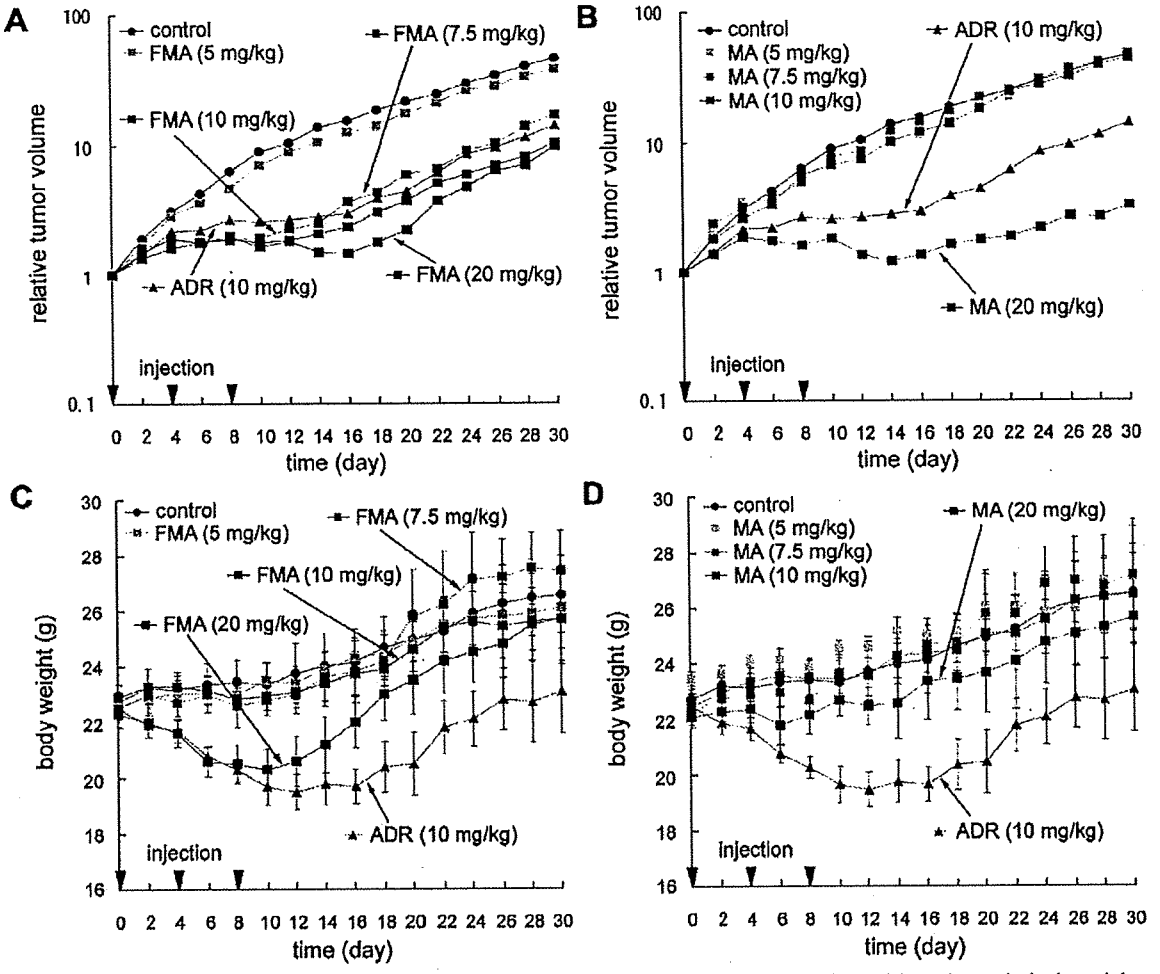

Figure 4. Tumor size and body weight change. The figure shows effective tumor-suppressing activity and low change in body weights over a broad range of injection doses of the folate-conjugated micelles (A and C). It clearly shows that the dose for effective tumor treatments decreased by folate conjugation compared to the micelles without folate, while toxicity remained lower than free drugs (B and D). Administrations were carried out 3 times with a 4 day interval into tumor-bearing CD-1 nude mice (female, 6-week-old, $n = 6$). The micelle doses are shown as ADR equivalents. Data are expressed as mean and mean ± SEM for relative and absolute values, respectively.

in the blood for a long time and their accumulation in tumor tissue increased significantly during the period of 24 h compared to normal organ. In the case of MA, the results correspond well with our previous data that revealed that the intracellular pH-sensitive micelles are characterized by prolonged circulation time in blood and tumor-specific accumulation (*19*). Such characteristic pharmacokinetic properties are considered to result from controlled drug release that can enhance the drug delivery efficiency of the micelles to the solid tumors. Regarding FMA, it is of interest that folate conjugation does not significantly affect the long-term circulation property of the micelles. FMA circulated in the blood for a prolonged time irrespective of folate content. However, the micelle accumulation in the liver as well as in the tumor changes obviously depending on the folate amount. As summarized in Table 4, a clear difference in tumor-specific accumulation was found between FMA and MA. The AUC values for each organ exhibit that FMA with a higher folate content showed a lower tumor-targeting property compared to MA. These results might be due to an increase in accumulation in the liver. Micelle accumulation in the liver was most probably due to the high FBP affinity of the micelles with increased folate concentration. In the meantime, the K_b values, which indicate the drug distribution within inter- and intracellular compartments, show that cellular uptake of FMA increased in tumor cells while remaining low in normal tissues. Nevertheless, the pharmacokinetic data also indicate that the possibility cannot be completely excluded that the micelles underwent nonspecific accumulation in normal organs after folate conjugation. It is not only because the K_b values increased, but also because the tumor to organ ratio (TOR) decreased as folate amounts increased. Accumulation in the liver increased, predominantly decreasing tumor-specific delivery efficiency. One of the previous studies showed that folate conjugation can induce higher hepatic clearance of the conjugates (*30*). Although expression of FBP in the liver would be suggested as a likely reason for the hepatic clearance, we considered that excessive conjugation of folate could increase accumulation of the micelles in normal organs. Therefore, it is concluded that the amount of folate should be carefully determined to facilitate tumor-targeting properties while maintaining long-term blood circulation. This would help us to minimize nonspecific distribution of the micelles in the body. Most noticeably, accumulation of the micelles in the tumor tissues did not significantly differ before and after folate conjugation in terms of pharmacokinetic profile. These findings indicate that the EPR effect seems to still be a major factor in determining the tumor accumulation of drug carriers for active targeting within a 24 h time range. In other words, folate conjugation would mainly affect the distribution of the micelles after extravasation rather than regulate migration of the micelles from the blood compartments to the tumor tissue.